HEAT & MASS TRANSFER

Third Edition
Supplemental Materials

A. F. Mills
Professor of Mechanical and Aerospace Engineering, Emeritus
The University of California at Los Angeles, Los Angeles, CA

C. F. M. Coimbra
Professor of Mechanical and Aerospace Engineering
The University of California at San Diego, La Jolla, CA

Temporal Publishing, LLC – San Diego, CA 92130

Library of Congress Cataloging-in-Publication Data

Mills, A. F. and Coimbra, C. F. M.
Heat and Mass Transfer Supplements 3/E by Anthony F. Mills & Carlos F. M. Coimbra
p. cm.
Includes bibliographical references and index.
ISBN 978-0-9963053-4-1
CIP data available.

Address inquiries or comments to:

contact@temporalpublishing.com www.temporalpublishing.com

Printed in the United States of America

10 9 8 7 6 5 4 3 2 1

ISBN 978-0-9963053-4-1

TEXT SUPPLEMENTS MILLS AND COIMBRA

OVERVIEW

A major problem facing authors of engineering textbooks is the selection of the topics to be covered. In established fields such as heat transfer, there is core material that all instructors expect to have covered in sufficient detail to provide students with a good learning experience. Then there is basic material on various topics that the instructors would like to have freedom to choose, as determined by the goals of the particular engineering program. Finally, there are new areas of heat and mass transfer science and technology that instructors might like to introduce to their students.

In preparing the 3rd editions of our textbooks we were faced by this problem. Our present coverage of heat and mass transfer is contained in the texts **Heat Transfer** and **Mass Transfer**, while reduced coverage is found in **Basic Heat Transfer** and **Basic Heat and Mass Transfer**. The latter two texts are intended for lower level courses. But the issue remained as to whether to remove some of the present material to accommodate the inclusion of new material. Most instructors agree that current engineering textbooks are at (or exceed) the size limit for practical use by students. Thus we have decided to take advantage of having a textbook website, which allows us to post supplementary material that is freely available to all. This approach allows us to continually update existing items, and to add new supplements as they come available.

The nature of our supplements varies. Some supplements have the purpose of providing more detailed explanations and clarifications of material in the texts. Examples include the supplements "Dimensional Analysis of Pipe Flow", "Dimensionless Groups for Viscous Dissipation" and "Flux Definitions for Mass Transport". New material is introduced in supplements such as "Flows in channels with Viscous Dissipation," "Flows with slip and Viscous Dissipation", and "Free Molecule Conduction". Supplements also give more examples of application of theory in the texts: energy balances at evaporating interfaces is an important topic in our mass transfer texts, and the supplement "The Ocean Surface Energy Balance" examines the issue for the ocean and its implications for global warming.

A special and very different supplement is "Error Analysis of Experiments," which is a manual originally prepared for students in the Mechanical and Aerospace Engineering Department at the University of California, Los Angeles. The unique feature of this manual is that the examples and case studies presented are almost all related to heat transfer, and many have a direct connection to material in our heat transfer texts. An unfortunate trend in educational programs has been to significantly reduce the laboratory experience that should accompany the study of subject, such as heat transfer. Students often commence major experimental research endeavors with negligible prior experience of the pitfalls that can be encountered in even the simplest of experiments. A good example is Case Study No. 5 that shows how often experimental results are falsified by errors in what was assumed to be a simple temperature measurement. Case study No. 6 provides an illustration of how a secondary or *nuisance* variable that is often ignored, can actually play an important role in a convective heat transfer experiment. Other case studies describe various lessons that were learnt building and testing heat transfer experiments in our laboratory: hopefully others might learn from our missteps!

We welcome suggestions from instructors for additional supplements that would augment our texts. Of course, feedback on the texts and website are also most welcome.

CONTENTS

SUPPLEMENT

1 DIMENSIONLESS GROUPS FOR VISCOUS DISSIPATION 1

References 5

2 FLOW IN CHANNELS WITH VISCOUS DISSIPATION 7

1 Introduction 8
2 Use of the Steady Flow Energy Equation (SFEE) 8
2.1 Model 1 – Incompressible Liquid 8
2.2 Model 2 – Perfect Gas 9
2.3 Model 3 – Pseudo-perfect gas [3, 4] 10
3 Fully Developed Temperature Profiles 10
3.1 Model 1. Incompressible Liquid 10
3.2 Model 2 – Perfect Gas 12
3.3 Low speed flow of a perfect gas 12
3.4 Model 3 – Pseudo-perfect gas I 14
3.5 Model 4 – Pseudo-perfect gas II 15
4 A Parallel Plate Heat Exchanger with Viscous Dissipation 16
References 18

3 FLOWS WITH SLIP AND VISCOUS DISSIPATION 21

1 Introduction 22
2 Couette Flow 22
2.1 Adiabatic Wall 24
2.2 Sample Calculation for Knudsen number $= 0.15$. 26
2.3 Comparison with Continuum Flow 26
3 Concluding Remarks 27
References 27

4 DISTRIBUTIONS OF MOLECULES AND PHOTONS 29

1 Molecular Distributions 30
2 Photon Distributions 33

5 FREE MOLECULE CONDUCTION 37

1 Introduction 38
2 Molecular Fluxes 38
3 Transport Between Infinite Parallel Black Walls 40

6 DIMENSIONAL ANALYSIS OF PIPE FLOW 45

7 FLUX DEFINITIONS FOR MASS TRANSPORT 53

1 Introduction 54
2 Mass and Molar Fluxes 54
3 Thermal Analogy to Mass Transport 56
4 Flaws in the Traditional Approach 56
5 Flow Model of Diffusion 57
6 Concluding Remarks 58
7 Acknowledgement 58
References 58

8 THE OCEAN SURFACE ENERGY BALANCE 61

1 Introduction 62
2 Temperature profiles in the tropical ocean 62
3 The energy balance at night 63
4 The energy balance in daytime 65
5 The transient problem 65
6 Solution of the balance equation 65
7 Effect of ocean temperature on heat loss 67
8 Effect of sky radiation on "heating" the ocean 69
9 Specification of the ocean surface temperature 72
10 The approximation $T_s = T_b$ 73
References 74

9 SOME MASS TRANSFER ISSUES CONCERNING COVID-19 75

1 Introduction 76
2 Droplet Evaporation and Deposition 76
3 Respirators and Masks 79
3.1 Respirators 79
3.2 Surgical Masks 80
3.3 Pressure Drop 80
3.4 Cloth Masks 81
3.5 The Epidemiology of Face Coverings for COVID-19 82
3.6 Recent Developments 84

3.7 Use of Two Masks 85
References 86

SUPPLEMENT

1

DIMENSIONLESS GROUPS FOR VISCOUS DISSIPATION

In the analysis of viscous dissipation effects on convective flows, we have introduced two dimensionless groups, namely the Eckert and Brinkman numbers. In Section 4.2.2 we considered *high speed flow* and recognize that kinetic energy can be converted into thermal energy to obtain the Eckert number

$$\mathrm{Ec} = \frac{(1/2)V^2}{c_p \Delta T} \tag{1}$$

The factor of 1/2 was introduced into the group arbitrarily to associate the group with kinetic energy. We went on to recognize that the conversion of kinetic energy into thermal energy is due to the action of viscous stresses, and yet viscosity does not appear in the Eckert number. So we chose alternative exponents to obtain the Brinkman number,

$$\mathrm{Br} = \frac{\mu V^2}{k \Delta T}$$

We also noted that these two groups are related as

$$\mathrm{Br} = 2\mathrm{Ec}\ \mathrm{Pr} \tag{2}$$

Subsequently in Section 5.2.1 we analyzed a Couette flow model of a high speed boundary layer flow. Equation (5.8) gave the temperature profile as

$$\frac{T_s - T}{T_s - T_e} = \frac{y}{L}\left[1 - \frac{\mu u_e^2}{2k(T_s - T_e)}\left(1 - \frac{y}{L}\right)\right] \tag{3}$$

and

$$\frac{\mu u_e^2}{2k(T_s - T_e)} = \frac{1}{2}\mathrm{Br} = \mathrm{Ec}\ \mathrm{Pr} = \frac{\frac{1}{2}u_e^2}{c_p(T_s - T_e)}\frac{c_p \mu}{k}$$

The $1/2u_e^2$ in EcPr is misleading since it suggests that kinetic energy is involved. But examination of Eq. (5.5) shows that the change in kinetic energy is actually zero, and the u_e^2 in Eq. (5.8) results from the square of the velocity gradient in the viscous dissipation term. Also, the specific heat c_p is not a parameter of the problem and hence neither is the Prandtl number.

Next we consider constant properties, fully developed laminar flow in a channel of width 2b with viscous dissipation, as in Exercise 5–9 in all our heat transfer texts, and in Exercise 5–44 of BHT, BHMT or Exercise 5–66 of HT. The energy equation is

$$\rho c u \frac{\partial T}{\partial x} = k\frac{\partial^2 T}{\partial y^2} + \mu\left(\frac{du}{dy}\right)^2 \tag{4}$$

For fully developed thermal conditions with a uniform wall heat flux, $\partial T/\partial x = dT_b/dx$, as shown for pipe flow in Section 5.3.2, and the right side of Eq. (4) is a constant. An energy balance on an element of channel dx long shows that

$$\frac{\partial T}{\partial x} = \frac{dT_b}{dx} = \frac{q_s}{\rho c u_b b} + \frac{3\mu u_b}{\rho c b^2} = \text{Constant} \tag{5}$$

Introducing dimensionless variables x^*, y^*, T^*, u^* such that

$$x = x^* L,\ y = y^* b,\ T = T_0 + (q_s b/k)T^*, \quad u = u^* u_b$$

where T_0 is the uniform inlet temperature (and will cancel), and following the analysis in Section 5.3.2 write $T^* - T_b^* = Y^*(y^*)$; then

$$\frac{\rho u_b c (q_s b/k)}{L}\frac{dT_b^*}{dx^*} = \frac{k(q_s b/k)}{b^2}\frac{d^2Y^*}{dy^{*2}} + \frac{\mu u_b^2}{b^2}\left(\frac{du^*}{dy^*}\right)^2$$

Dividing by $k(q_s b/k)/b^2$ then gives

$$\mathrm{Gz}\, u^* \frac{dT_b^*}{dx^*} = \frac{d^2Y^*}{dy*^2} + \mathrm{Br}^*\left(\frac{du^*}{dy^*}\right)^2 \tag{6}$$

where $\mathrm{Br}^* = \mu u_b^2/q_s b$ is an alternative form of the Brinkman number that is useful for a uniform wall heat flux, and $\mathrm{Gz} = b^2 u_b/\alpha L$ is a Graetz number, which was introduced in Section 5.6.1 of HT and Eq. (4.50) of all the heat transfer texts. The Nusselt number is

$$\mathrm{Nu}_{D_h} = \frac{h_c(4b)}{k} = \frac{q_s(4b)}{k(T_s - T_b)} = \frac{4}{(T_s^* - T_b^*)} \tag{7}$$

Since dT_b^*/dx^* is a constant, Eq. (6) is an ordinary differential equation for $Y^*(y^*)$, and contains only one dimensionless parameter, Br^*. Thus,

$$\mathrm{Nu}_{D_h} = f(\mathrm{Br}^*) \tag{8}$$

The analysis in Supplement 2 shows that the actual result is

$$\mathrm{Nu}_{D_h} = \frac{140/17}{1 + (27/17)\mathrm{Br}^*} \tag{9}$$

confirming our scaling analysis.

Lastly we consider the laminar boundary layer on a flat plate, for which the thermal energy equation has the form

$$\rho u c\frac{\partial T}{\partial x} + \rho v c\frac{\partial T}{\partial y} = k\frac{\partial^2 T}{\partial y^2} + \mu\left(\frac{\partial u}{\partial y}\right)^2 \tag{10}$$

Equation (10) applies to an incompressible liquid for which $c_p = c_v = c$, and also applies to an ideal gas with $c = c_p$; both cases for constant ρ, k and μ.

Following the procedure in Section 5.8.1 of HT, we choose dimensionless variables such that $T = T^*(T_s - T_e) + T_e$, $x = x^* L$, $y = y_T^* \Delta$, $u = u^* V$, $v = v^*(\delta/L)V$. Then

$$\frac{\rho c(T_s - T_e)V}{L}\left(u^*\frac{\partial T^*}{\partial x^*} + \frac{\delta}{\Delta}v^*\frac{\partial T^*}{\partial y_T^*}\right) = \frac{k(T_s - T_e)}{\Delta^2}\left(\frac{\partial^2 T^*}{\partial y_T^{*2}}\right) + \frac{\mu V^2}{\Delta^2}\left(\frac{\partial u^*}{\partial y_T^*}\right)^2 \tag{11}$$

Divide by $\rho c(T_s - T_e)V/L$.

$$u^* \frac{\partial T^*}{\partial x^*} + \frac{\delta}{\Delta} v^* \frac{\partial T^*}{\partial y_T^*} = \frac{1}{\mathrm{RePr}} \frac{L^2}{\Delta^2} \left[\left(\frac{\partial^2 T^*}{\partial y_T^{*2}} \right) + \mathrm{Br} \left(\frac{\partial u^*}{\partial y^*} \right)^2 \right] \tag{12}$$

But $\dfrac{\delta}{L} = \dfrac{1}{\mathrm{Re}^{1/2}}$, so $\dfrac{1}{\mathrm{Re\,Pr}} \dfrac{L^2}{\Delta^2} = \dfrac{1}{\mathrm{Pr}} \dfrac{\delta^2}{\Delta^2}$, and

$$u^* \frac{\partial T^*}{\partial x^*} + \frac{\delta}{\Delta} v^* \frac{\partial T^*}{\partial y_T^*} = \frac{1}{\mathrm{Pr}} \frac{\delta^2}{\Delta^2} \left[\frac{\partial^2 T^*}{\partial y_T^*} + \mathrm{Br} \left(\frac{\partial u^*}{\partial y_T^{*2}} \right)^2 \right] \tag{13}$$

The wall heat flux and Nusselt numbers are

$$q_s = -k \left. \frac{\partial T}{\partial y} \right|_0 = \frac{-k(T_s - T_e)}{\Delta} \left. \frac{\partial T^*}{\partial y_T^*} \right|_0$$

$$Nu = \frac{q_s L}{(T_s - T_e)k} = \frac{L}{\Delta} \left. \frac{\partial T^*}{\partial y_T^*} \right|_0 = \mathrm{Re}^{1/2} \frac{\delta}{\Delta} \frac{\partial T^*}{\partial y_T^*} \tag{14}$$

The dimensional parameters in Eq. (13) are δ/Δ, Pr, Br. From results for no dissipation given in Section 5.8.1 of HT, we expect δ/Δ to be a function of Pr, but this ratio may also depend on Br. Nevertheless, we can assert that Pr and Br are the only independent dimensionless parameters in Eq. (13) and write

$$Nu = Re^{1/2} f(Pr, Br) \tag{15}$$

Of particular interest is the solution for Nu = 0, which gives the **adiabatic wall temperature** T_{aw}. Section 5.1 of our texts we show how replacing T_e by T_{aw} allows correlations for low speed flows to be extended to high speed flows. The *recovery factor* is defined by

$$T_{aw} = T_e + r \frac{u_e^2}{2c_p}$$

$$\text{or } r = \frac{u_e^2}{2c_p(T_{aw} - T_e)} = Ec_{aw} = \frac{Br_{aw}}{2Pr} \tag{16}$$

The recovery factor is used mainly in connection with supersonic and hypersonic air boundary layers and aerospace engineers have historically used the Eckert number Ec rather than Br/Pr for their analyses. An advantage of using the Eckert number for fluids in general is that then Eq. (15) can be used in the form

$$Nu = Re^{1/2} f(Ec, Pr) \tag{17}$$

so that the properties k and μ are combined in one group only, and it is these properties that vary greatly from one fluid to another.

For an adiabatic wall, Nu = 0, so from Eq. 17, $f(Ec_{aw}, Pr) = 0$. If the function is of the form,

$$Ec_{aw} - g(Pr) = 0$$

then from Eq. (16), $g(Pr) = r$ the recovery factor. From the Nusselt number dependence on Pr without dissipation given in Section 5.8 of HT, we expect the limit forms

$$Pr \to 0; \quad r \sim Pr^{1/2} \tag{18a}$$

$$Pr \to \infty; \quad r \sim Pr^{1/3} \tag{18b}$$

Table 1 which follows gives the results of the exact numerical solution required as Exercise 5–36 of HT.

Table 1

Pr	r	$Pr^{1/2}$	$1.9Pr^{1/3}$	Eq. (19)
0.01	0.09434	0.1000	-	-
0.03	0.1652	0.1732	-	-
0.10	0.3073	0.3163	-	-
0.72	0.8477	0.8485	-	-
1.00	1.000	1.000	1.900	0.998
3.00	1.709	1.732	2.740	1.659
10.00	2.962	3.162	4.094	2.901
30.00	4.724	5.477	5.904	4.685

Over the range $0.01 < \mathrm{Pr} < 10$, $r = \mathrm{Pr}^{1/2}$ is a good approximation. The large Pr asymptote of $1.9\mathrm{Pr}^{1/3}$ is not satisfactory at $Pr = 30$. The interpolation formula developed by Narasimha and Vasantha [1],

$$r = 1.922(\mathrm{Pr} + 0.805)^{1/3} - 1.341 \tag{19}$$

is seen to work well for $\mathrm{Pr} = 1$ to 30 and will be more accurate at higher Pr values. The high Prandtl number result is of practical relevance since viscous dissipation can cause a large difference between T_{aw} and T_e for oils: on the other hand, the low Prandtl number limit is of little practical interest, since for these liquid metals the difference between T_{aw} and T_e is very small and viscous dissipation effects are small and can be ignored. Accurate values for r at low Pr values do not appear to be available.

REFERENCES

1. Narasimha, R., and Vasantha, S., "Laminar boundary layer on a flat plate at high Prandtl number." *Z. angew. Math, Phys. (ZAMP) Bd 17,* 585–592 (1966).

SUPPLEMENT

2

FLOW IN CHANNELS WITH VISCOUS DISSIPATION

CONTENTS

1 Introduction 8
2 Use of the Steady Flow Energy Equation (SFEE) 8
2.1 Model 1 – Incompressible Liquid 8
2.2 Model 2 – Perfect Gas 9
2.3 Model 3 – Pseudo-perfect gas [3, 4] 10
3 Fully Developed Temperature Profiles 10
3.1 Model 1. Incompressible Liquid 10
3.2 Model 2 – Perfect Gas 12
3.3 Low speed flow of a perfect gas 12
3.4 Model 3 – Pseudo-perfect gas I 14
3.5 Model 4 – Pseudo-perfect gas II 15
4 A Parallel Plate Heat Exchanger with Viscous Dissipation 16

1 INTRODUCTION

Our heat transfer texts contain introductory material on heat transfer in flows with viscous dissipation. Section 5.2 of HT, BHT and BHMT presents an analysis of incompressible Couette flow to give a *recovery factor* $r = \mathrm{Pr}$, which allows the *adiabatic wall temperature* to be calculated. The result was extended to laminar and turbulent boundary layers by giving empirical expressions for r, namely $\mathrm{Pr}^{1/2}$ and $\mathrm{Pr}^{1/3}$ respectively. Section 5.7.3 of HT presents a derivation of the general energy conservation equation, including the *dissipation* function.

A number of exercises involve viscous dissipation. Exercise 5–1 through 5–6 are based on Section 5.2. Exercises 5–9, 5–11 and 5–21 all consider incompressible flow in channels, as do 5–44 of BHT and BHMT, and 5–66 of HT. Exercise 5–18 considers high speed air flow in a microtube for which compressibility is also considered. Finally, Exercise 5–36 of HT requires the solution of the self similar constant property laminar boundary equations involving viscous dissipation: the result was a correlation of the recovery factor $r \simeq \mathrm{Pr}^{1/2}$.

The research literature contains many papers that investigate the effect of viscous dissipation in laminar tube and channel flow. Recent work has been motivated by current interest in technologies that involve flow in microchannels.

2 USE OF THE STEADY FLOW ENERGY EQUATION (SFEE)

It is instructive to first apply the steady flow energy equation of thermodynamics in a slightly different form to Eq. (1.4) of the texts. With negligible change of potential energy and no external work, the SFEE can be written as

$$\dot{m}\Delta\left(h_b + a_0\frac{u_b^2}{2}\right) = \dot{Q} \tag{1}$$

where the subscripts b denotes bulk values, and a_0 results from proper averaging of kinetic energy across the channel. Exercise 5–16 requires the determination of a_0 for various flows: for laminar flow between parallel plates $a_0 = 1.544$. Equation (1) will be applied to various models of real fluids.

2.1 Model 1 – Incompressible Liquid

It is useful to simply consider an adiabatic channel so $\dot{Q} = 0$. Then for constant ρ there is no change in kinetic energy and

$$dh_b = 0 \tag{2}$$

or

$$cdT_b + \frac{dp}{\rho} = 0; \quad c = c_v \tag{3}$$

and

$$\frac{dT_b}{dx} = \frac{1}{\rho c}\left(-\frac{dp}{dx}\right) \tag{4}$$

For laminar flow in a channel of width 2b, the pressure gradient is (Exercise 5.8)

$$\frac{dp}{dx} = -\frac{3\mu u_b}{b^2} \tag{5}$$

hence,

$$\frac{dT_b}{dx} = \frac{3\mu u_b}{\rho c b^2} \tag{6}$$

Equation (6) gives the increase in T_b along the channel due to viscous dissipation. Notice that it is the work done by the pressure force that is ultimately converted into thermal energy by viscous dissipation. To illustrate this point Eq. (4) can be rewritten

$$\rho c u_b \frac{dT_b}{dx} = u_b\left(-\frac{dp}{dx}\right) \tag{7}$$

which shows how the rate at which internal energy is gained by the fluid is related to the rate at which work is done on the fluid by the pressure force.

2.2 Model 2 – Perfect Gas

Again consider an adiabatic channel, $\dot{Q} = 0$, but now ρ is not constant so u_b and kinetic energy can change along the channel,

$$dh_b + d\left(a_0 \frac{u_b^2}{2}\right) = 0 \tag{8}$$

Case (i) Low Speed flow

For low speed flow, accelerations are small and we take the change in kinetic energy as negligible. Then

$$dh_b = c_p dT_b \simeq 0$$

and

$$\frac{dT_b}{dx} \simeq 0, \quad T_b \simeq \text{constant} \tag{9}$$

The heat generated by viscous dissipation now equals the heat absorbed in the expansion of the gas.

Case (ii) High Speed flow

If accelerations are not small, the change in kinetic energy is not negligible. Then for an adiabatic wall we have the approximate solution of Fanno flow found in gas dynamics texts [1, 2].

$$\frac{dT_b}{dx} = -\frac{\gamma(\gamma-1)M^4}{2(1-M^2)}\frac{fT_b}{2b}. \tag{10}$$

The temperature gradient is now negative, not zero as for low speed flow. The increase in kinetic energy requires more work and a higher pressure gradient: the density decrease is then larger and the expansion cooling now becomes larger than the viscous heating.

2.3 Model 3 – Pseudo-perfect gas [3,4]

A number of papers have appeared in the literature where a perfect gas is assumed to write $dh = c_p dT$, but otherwise properties ρ, μ, k are assumed constant. Then for an adiabatic channel Eq. (1) again gives

$$dh_b = 0$$

so

$$c_p dT_b = 0, \quad \text{or} \quad \frac{dT_b}{dx} = 0. \tag{11}$$

which is identical to Eq. (9) for low speed flow of a perfect gas. Thus the assumption of constant density is equivalent to postulating a low speed flow for Model 2 when using the steady flow energy equation

Viscous heating plays an important role in some flows of viscoelastic fluids, for example in the extrusion of polymers. However, viscoelastic fluids are beyond the scope of our texts.

3 FULLY DEVELOPED TEMPERATURE PROFILES

Next we present temperature profiles for fully developed conditions: details of the derivations are left to the student as exercises.

3.1 Model 1. Incompressible Liquid

The governing thermal energy equation is obtained from Eq. (5.209) of HT with μ and k constant,

$$\rho c u \frac{\partial T}{\partial x} = k \frac{\partial^2 T}{\partial y^2} + \mu \left(\frac{\partial u}{\partial y} \right)^2 \tag{12}$$

Solution for an adiabatic wall:

$$T - T_c = \frac{9 \mu u_b^2}{8k} \left[2 \left(\frac{y}{b} \right)^2 - \left(\frac{y}{b} \right)^4 \right] \tag{13}$$

$$T_{aw} - T_b = \frac{27}{35} \frac{\mu u_b^2}{k} \tag{14}$$

$$\frac{dT_b}{dx} = \frac{3 \mu u_b}{\rho c b^2} \tag{15}$$

where Eq. (15) agrees with Eq. (6) derived from the steady flow energy equation.

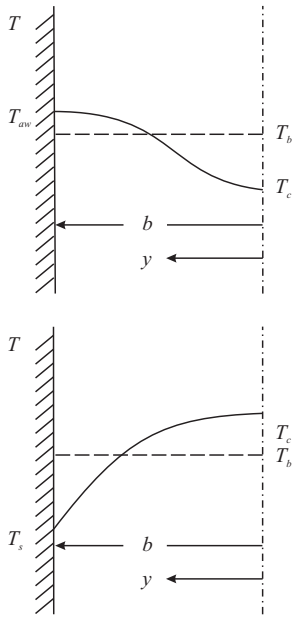

Solution for uniform wall temperature.

$$T - T_s = \frac{3}{4}\frac{\mu u_b^2}{k}\left[1 - \left(\frac{y}{b}\right)^4\right] \tag{16}$$

$$T_b - T_s = \frac{24}{35}\frac{\mu u_b^2}{k} \tag{17}$$

$$\frac{dT_b}{dx} = 0 \tag{18}$$

$$Nu_{D_h} = \frac{q_s(4b)}{k(T_s - T_b)} = 17.5 \tag{19}$$

Solution for uniform wall heat flux.

$$T - T_c = \frac{q_s b}{8k}\left[6\left(\frac{y}{b}\right)^2 - \left(\frac{y}{b}\right)^4\right] + \frac{9}{8}\frac{\mu u_b^2}{k}\left[2\left(\frac{y}{b}\right)^2 - \left(\frac{y}{b}\right)^4\right] \tag{20}$$

$$T_s - T_b = \frac{17}{35}\frac{q_s b}{k} + \frac{27}{35}\frac{\mu u_b^2}{k} \tag{21}$$

$$Nu_{D_h}^{(1)} = \frac{q_s(4b)}{k(T_s - T_b)} = \frac{140/17}{1 + \frac{27}{17}Br^*}; \tag{22}$$

$$Nu_{D_h}^{(2)} = \frac{q_s(4b)}{k(T_s - T_{aw})} = \frac{140}{17} = 8.235 \tag{23}$$

$$\frac{dT_b}{dx} = \frac{q_s}{\rho c u_b b} + \frac{3\mu u_b}{\rho c b^2} \tag{24}$$

$\mathrm{Nu}_{D_h}^{(1)}$ is the usual Nusselt number based on $(T_s - T_b)$; $\mathrm{Nu}_{D_h}^{(2)}$ is based on $(T_s - T_{aw})$,

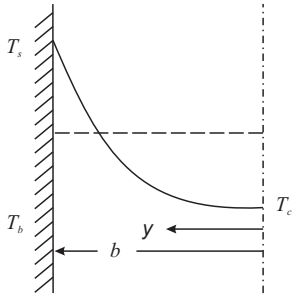

and is the same as for the solution for no dissipation. Recall that Section 5.3 of our texts gives the corresponding solution for a circular tubes. Equation (23) is also given in Table 4.5 of the texts. Equation (12) is a linear differential equation so that this solution can be obtained by superposition of a solution for a uniform wall heat flux with no dissipation, and a solution for an adiabatic wall with dissipation. Notice that the Brinkman number in Eq. (22) is defined in Supplement No. 1 as $\mathrm{Br}^* = \mu u_b^2/q_s b$, and differs from the one defined in Sections 4.2.2 and 5.2.1 of our texts. Examination of Eq. (5.9) shows how the two definitions are related.

3.2 Model 2 – Perfect Gas

For a perfect gas with variable properties the governing equations are obtained from Eqs. (5.192), (5.194a) and (5.208) of HT, together with the equation of state.

$$P = \rho RT \tag{25}$$

$$\frac{\partial}{\partial x}(\rho u) + \frac{\partial}{\partial y}(\rho u) = 0 \tag{26}$$

$$\rho u\frac{\partial u}{\partial x} + \rho v\frac{\partial u}{\partial y} = -\frac{dP}{dx} + \frac{\partial}{\partial y}\left(\mu\frac{\partial u}{\partial y}\right) \tag{27}$$

$$\rho u c_p\frac{\partial T}{\partial x} + \rho v c_p\frac{\partial T}{\partial y} = u\frac{dP}{dx} + \frac{\partial}{\partial y}\left(k\frac{\partial T}{\partial y}\right) + \mu\left(\frac{\partial u}{\partial y}\right)^2 \tag{28}$$

For fully developed conditions these equations invoke the assumption of negligible momentum changes across the channel (much like the boundary layer assumptions for a thin boundary layer). Numerical solutions are required to solve this equation set.

3.3 Low speed flow of a perfect gas

If fluid acceleration is neglected and properties including ρ, μ, k are assumed constant, the momentum equation may be solved to obtain the result for incompressible flow, the planar channel equivalent of Pousiulle flow as analyzed in Exercise 5.8 of

our texts. The energy equation becomes

$$\rho c_p u \frac{\partial T}{\partial x} = u\frac{dP}{dx} + k\frac{\partial^2 T}{\partial y^2} + \mu\left(\frac{du}{dy}\right)^2 \tag{29}$$

From Exercise (5.8),

$$u = \frac{3}{2}u_b\left(1-\left(\frac{y}{b}\right)^2\right); \quad \frac{dP}{dx} = -\frac{3\mu u_b}{b^2}; \quad \left(\frac{du}{dy}\right)^2 = \frac{9u_b^2}{b^2}\left(\frac{y}{b}\right)^2 \tag{30}$$

Substituting in Eq. (29) gives

$$\rho c_p u \frac{\partial T}{\partial x} = k\frac{\partial^2 T}{\partial y^2} + \frac{9}{2}\frac{\mu u_b^2}{b^2}\left(3\left(\frac{y}{b}\right)^2 - 1\right) \tag{31}$$

Solution for a uniform wall heat flux (UHF): Using the SFEE:

$$\frac{dT_b}{dx} = \frac{q_s}{\rho c_p u_b b} = \frac{\partial T}{\partial x} \tag{32}$$

(33)

Substituting in Eq. (31) and solving the resulting ordinary differential equation gives

$$T_s - T_b = \frac{17}{35}\frac{q_s b}{k} + \frac{27}{35}\frac{\mu u_b^2}{k} \tag{34}$$

$$Nu = \frac{q_s(4b)}{k(T_s - T_b)} = \frac{140/17}{1+\frac{27}{17}Br^*} \tag{35}$$

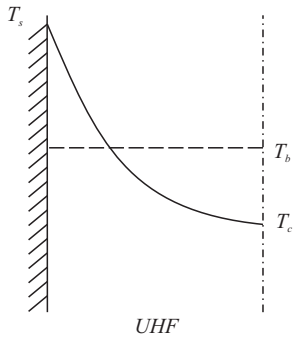

Solution for a uniform wall temperature (UWT): Substituting $\partial T/\partial x = 0$ in Eq. (31) and solving gives

$$T - T_s = -\frac{9}{8}\frac{\mu u_b^2}{k}\left(1 - \left(\frac{y}{b}\right)^2\right)^2 \tag{36}$$

$$T_b - T_s = -\frac{27}{35}\frac{\mu u_b^2}{k} \tag{37a,b}$$

$$q_s = -k\frac{\partial T}{\partial y}|_s = 0, \text{ hence } Nu = 0 \tag{37}$$

Thus a solution for $\partial T/\partial x = 0$ gives a wall that is both isothermal and adiabatic.

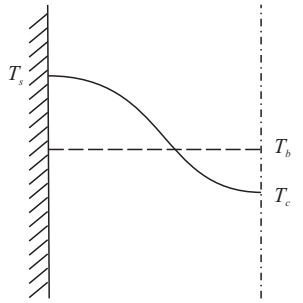

UWT

The fully developed solution for UHF is identical to that for an incompressible liquid, for example, compare Eqs. (22) and (35). However, for UWT they are different: Eq. (36) gives Nu = 0, whereas Eq. (19) gives $\text{Nu}_{D_h} = 17.5$. For the perfect gas the solution is one that balances viscous dissipation against expansion cooling to give zero heat transfer, $q_s = 0$, in accord with Eq. (9) for the SFEE applied to a perfect gas.

3.4 Model 3 – Pseudo-perfect gas I

The pseudo-perfect gas was used by Ou and Chang [3] and Hadjconstantinou [4]. The relationship $dh = c_p dT$ is assumed and otherwise ρ, μ and k are assumed constant. The governing thermal energy equation is obtained from Eq. (5.208) as

$$\rho u c_p \frac{\partial T}{\partial x} = u\frac{dP}{dx} + k\frac{\partial^2 T}{\partial y^2} + \mu\left(\frac{du}{dy}\right)^2 \tag{38}$$

This equation differs from Eq. (17) for an incompressible liquid in that c_p rather than c_v appears in the convective term. Equation (38) is identical to Eq. (29) for low speed flow: the assumptions of constant density and low-speed flow are equivalent.

The role played by the term udP/dx in Eq. (38) has been the source of some confusion. Equation (12) for incompressible flow has no such term. This term is called "flow work" in References [3, 4]. Equation (38) is derived from the thermal energy equation, Eq. (5.205) of HT, by eliminating internal energy in favor of enthalpy, and then assuming a perfect gas to write $dh = c_p dT$. In the process, the reversible work

done by the pressure gradient, $-Pdu/dx$, is absorbed in the enthalpy change, as is the irreversible work done by the pressure gradient to maintain the flow, udP/dx. Thus udP/dx has to be subtracted from the left side of the equation, and appears as an addition on the right side. Clearly, udP/dx is not the flow work of thermodynamics, but rather the negative of the portion required to overcome viscous stresses. At first sight, the appearance of a work term udP/dx in a thermal energy equation is unexpected: but as shown above, it is an artifice that cancels an identical term on the left side of the equation.

Looking at Eq. (38) we can note that the term udP/dx is negative, is zero at the walls and a minimum at the centerplane. The term $\mu(du/dy)^2$ is positive and is a maximum at the walls and zero at the centerplane. The term udP/dx acts as a thermal energy sink, while $\mu(du^2/\partial y)^2$ is a source: thus T is a maximum at the walls and a minimum at the centerplane. Using Eqs. (30), we can integrate across the duct to obtain

$$\int_{-b}^{+b} u\frac{dP}{dx} = u_b 2b\frac{dP}{dx} = -\frac{6\mu u_b^2}{b} \tag{39}$$

$$\int_{-b}^{+b} \mu\left(\frac{du}{dy}\right)^2 = +\frac{6\mu u_b^2}{b} \tag{40}$$

This integrated sink and source balance is a result expected from the steady flow energy equation applied to an adiabatic channel for a perfect gas and negligible changes in kinetic energy: from Eq. (11), $dT_b/dx = 0$.

3.5 Model 4 – Pseudo-perfect gas II

This model is found in Bird, Stewart and Lightfoot [5], and again takes $dh = c_p dT$ and assumes properties are otherwise constant; but in addition the term $u\,dP/dx$ is neglected. The governing equation is then

$$\rho c_p u\frac{\partial T}{\partial x} = k\frac{\partial T}{\partial y^2} + \mu\left(\frac{du}{dy}\right)^2 \tag{41}$$

Solution for an adiabatic wall:

First integrate Eq. (41) across the channel,

$$\rho c_p u_b b\frac{dT_b}{dx} = \frac{3\mu u_b^2}{b}$$

or

$$\frac{dT_b}{dx} = \frac{3\mu u_b}{\rho c b^2} \tag{42}$$

which is the same as Eq. (6) for an incompressible liquid. However, Eq. (9) for low speed flow of a perfect gas gives $dT_b/dx = 0$, so this model violates the steady flow energy equation. With this inconsistency it is doubtful in the model has much utility.

4 A PARALLEL PLATE HEAT EXCHANGER WITH VISCOUS DISSIPATION

In Section 3 we have presented analyses of fully developed heat transfer in duct flows for various fluids. Such convection analyses allow us to gain an understanding of the basic physics of the flows. However, for engineering application, we need to understand the possible consequences of viscous dissipation on the performance of heat exchangers, in particular microscale heat exchangers. Thus we now extend the heat exchanger analysis in Chapter 8 to include the effect of viscous dissipation.

In Chapter 8 we used the steady flow energy equation of thermodynamics to derive the governing differential equations. Now we have two choices, the SFEE, or the governing partial differential equation for flow with viscous dissipation used in Section 3: for simplicity we will use the SFEE and comment on the alternative approach when pertinent. Thus we will start with Eq. (1) of this supplement and consider an incompressible liquid so as to have no change in kinetic energy; then

$$\dot{m} dh_b = d\dot{Q} \tag{43}$$

substituting $h_b = cT_b + \frac{P}{\rho}$, and dividing by dx,

$$\dot{m}c\frac{dT_b}{dx} + \frac{\dot{m}}{\rho}\frac{dP}{dx} = \frac{d\dot{Q}}{dx}; \quad d\dot{Q} = q_s \mathscr{P} dx$$

or

$$\frac{dT_b}{dx} = -\frac{1}{\rho c}\frac{dP}{dx} + \frac{q_s \mathscr{P}}{\dot{m}c} \tag{44}$$

Alternatively we could start with Eq. (12) and integrate it across the duct to obtain

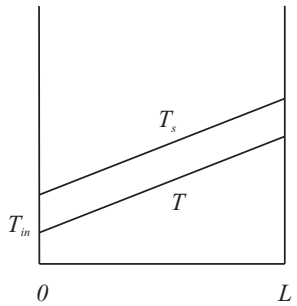

$$\dot{m}c\frac{dT_b}{dx} = \frac{6\mu u_b^2}{b} + q_s \mathscr{P}$$

or

$$\frac{dT_b}{dx} = \frac{6\mu u_b^2}{\dot{m}cb} + \frac{q_s \mathscr{P}}{\dot{m}c} \tag{45}$$

Since $\frac{dP}{dx} = -\frac{3\mu u_b}{b^2}$ and $\dot{m} = \rho u_b (2b)$, Eqs. (44) and (45) are equivalent. One might think that Eq. (45) would be preferable for our purpose since it contains the viscous dissipation term in its usual form, whereas Eq. (44) contains the work done by the

pressure gradient that supports the dissipation. However, for heat exchanger design, pressure drop is an important factor, and can even be a limiting constraint. See Chapter 8, Section 8.6 and Exercises 8.89 and 8.89 of HT (8.89 and 8.90 of BHT, BHMT). Silicon wafer based structures used for microelectronic cooling may have a pressure limit of ~ 2 atm gage.

Integrating Eq. (44) and using HX notation to drop the subscript b,

$$T_{\text{out}} - T_{\text{in}} = \frac{P_{\text{in}} - P_{\text{out}}}{\rho c} + \frac{q_s \mathscr{P} L}{\dot{m} c} \tag{46}$$

If axial conduction can be neglected, cooling of electronics components is characterized by a uniform heat flux along the coolant path:

$$\begin{aligned} q_s &= \text{constant} \\ &= h_c(T_s - T), \text{ thus} \\ q_s &= h_c(T_{s,L} - T_{\text{out}}) \end{aligned} \tag{47}$$

Let $N_{tu} = \frac{h_c \mathscr{P} L}{\dot{m} c}$, then

$$T_{\text{out}} - T_{\text{in}} = N_{tu}(T_{s,L} - T_{\text{out}}) + \frac{\Delta P}{\rho c}$$

$$T_{\text{out}} = T_{\text{in}} + N_{tu} T_{s,L} - N_{tu} T_{\text{out}} + \frac{\Delta P}{\rho c}$$

$$T_{\text{out}}(1 + N_{tu}) = T_{\text{in}} + N_{tu} T_{s,L} + \frac{\Delta P}{\rho c}. \tag{48}$$

$$T_{\text{out}} = \frac{T_{\text{in}} + N_{tu} T_{s,L} + \Delta P/\rho c}{1 + N_{tu}} \tag{49}$$

$$T_{s,L} - T_{\text{out}} = \frac{(T_{s,L} - T_{\text{in}}) - \Delta P/\rho c}{1 + N_{tu}} \tag{50}$$

The total heat transfer in the channel is

$$\begin{aligned} \dot{Q} &= h_c(T_{s,L} - T_{\text{out}}) \mathscr{P} L; \quad \mathscr{P} = 2W \\ &= \frac{h_c \mathscr{P} L}{1 + N_{tu}} [(T_{s,L} - T_{\text{in}}) - \Delta P/\rho c] \\ \dot{Q} &= \frac{N_{tu}}{1 + N_{tu}} \dot{m} c [(T_{s,L} - T_{\text{in}}) - \Delta P/\rho c] \end{aligned} \tag{51}$$

In cooling electronic gear there a temperature limit to ensure an acceptable lifetime of the components. Thus we set $T_{s,L} = T_{\max}$

$$\dot{Q} = \frac{N_{tu}}{1 + N_{tu}} \dot{m} c \left[(T_{\max} - T_{\text{in}}) - \frac{\Delta P}{\rho c}\right] \tag{52}$$

In the limit of negligible viscous dissipation, $\dot{m} c (T_{\max} - T_{\text{in}})$ is the maximum heat transfer attainable: the ratio $N_{tu}/(1 + N_{tu})$ is the actual fraction of the maximum that

is attained. Thus $N_{tu}/(1+N_{tu})$ can be viewed as the effectiveness of the exchanger. The ratio $N_{tu}/(1+N_{tu})$ varies from 0.5 to 0.8 as N_{tu} increases from 1 to 4. A value of N_{tu} much larger than 4 would probably not be cost effective.

Turning now to examine the effects of viscous dissipation we see the important role played by a pressure drop constraint. For example consider a silicon wafer-structure with a structural limit of 2 atm. gage. Using Dowtherm A as a possible coolant gives applicable property values of $\rho = 1000$ kg/m^3, $c = 1600$ J/kg K. Thus $\Delta P/\rho c = (2\times 10^5)/(1000)(1600) = 0.125$ K. Typically $T_{\max} = 90^\circ$C may be specified; for $T_{\text{in}} = 30^\circ$C, $\Delta T = 60$K. Since $0.125 \ll 60$, the first order effect of dissipation is negligible.

Viscous dissipation also affects the temperature profile across the channel and hence the Nusselt number. Equation (22) of Supplement 2 gave

$$Nu_{D_h} = \frac{q_s(4b)}{(T_s - T_b)} = \frac{140/17}{1+\frac{27}{17}Br^*}; \quad Br^* = \frac{\mu u_b^2}{q_s b}$$

Let us assume Br* is small for a first iteration. Then $Nu_{D_h} = 140/17$, $h_c = (140/17)k/4b$ and $q_s b \simeq 2k\Delta T$. Also, $\Delta P = (3\mu u_b/b^2)L$ and $u_b = \Delta P b^2/3\mu L$, thus

$$Br^* = \frac{(\Delta P)^2 b^4}{18\mu L^2 k\Delta T} \tag{53}$$

To estimate ΔT, take $T_{\text{in}} = 30^\circ$C, $T_{\max} = 90^\circ$C, $\varepsilon = 0.8$. Then $T_{\text{out}} = 78^\circ$C and $\Delta T =$ 12 K, (and is constant along the exchanger). Using $\mu = 1.6\times 10^{-3}$ kg/m s and $k =$ 0.14 W/m K, Br* can be evaluated as $Br^* = \frac{(2\times 10^5)^2(5\times 10^{-5})^4}{(18)(1.6\times 10^{-3})(0.01)^2(0.14)(12)} = 5.17\times 10^{-4}$, and $(27/17)Br^* = 8.2\times 10^{-4} \ll 1$. So clearly the Brinkman number is too small to have any significant effect on Nusselt number. Thus we can conclude that for cooling of silicon-wafer based structures for microelectronic devices, the effect of viscous dissipation on thermal performance is quite negligible. It is the severe pressure drop constraint that is the cause of this result.

Although we have used a parallel plate duct for our analysis, the conclusion with regards to viscous dissipation applies to ducts of any aspect ratio, and for circular tubes.

Comment

Notice that the effectiveness of this exchanger, $N_{tu}/(1+N_{tu})$ is the same as for a balanced flow counter flow exchanger, as given by Eq. (8.45). The reason for this identical result is that both heat exchangers are characterized by a constant heat transfer along the exchanger, and hence a constant ΔT.

REFERENCES

1. Wikipedia entry for Fanno flow.
2. Shapiro, A.H. *The Dynamics and Thermodynamics of Compressible Fluid Flow*, Volume 1, Ronald Press, 1953.

3. Ou, J.-W. and Cheng, K.C. "Effect of pressure work and viscous dissipation on Graetz problem for gas flows in parallel-platechannels" Warme-und-Stoffubertragung 6, 191–198 (2003).

4. Hadjiconstantinou, N.G., "Dissipation in small scale gaseous flows". J. Heat Transfer 125, 944–947 (2003).

5. Bird, R.B., Stewart, W. and Lightfoot, E.N. *Transport Phenomena*, revised 2nd ed., John Wiley and Sons, New York (2006).

SUPPLEMENT

3

FLOWS WITH SLIP AND VISCOUS DISSIPATION

CONTENTS

1 Introduction 22
2 Couette Flow 22
2.1 Adiabatic Wall 24
2.2 Sample Calculation for Knudsen number = 0.15. 26
2.3 Comparison with Continuum Flow 26
3 Concluding Remarks 27

1 INTRODUCTION

When a gas flow becomes slightly rarefied, that is the Knudsen number λ/L is small, but not zero, say $Kn < 0.1 - 0.2$, the slip flow model is used for analysis. The gas is imagined to have a slip velocity u_s at the edge of a thin "Knudsen layer" adjacent to a wall, of thickness order λ. The slip velocity is written

$$u_s = \alpha\lambda \frac{du}{dy}\Big|_s \tag{1}$$

where α is a constant close to unity and depends on the nature of collisions between the molecules and the wall. In slip flow there is also a temperature "jump" at the wall,

$$\Delta T_s = \alpha_T \frac{2\gamma}{\gamma+1}\frac{\lambda}{Pr}\frac{dT}{dy}\Big|_s \tag{2}$$

where α_T is a thermal accomodation coefficient, also close to unity.

Early interest in slip flows was related to flight in the upper atmosphere, and flows in vacuum equipment. Recently there has been renewed interest in connection with flows for cooling microelectronic devices. The slip flow regime is encountered because of small passage sizes, not due to low pressure levels. In addition, the flow rates required result in values of Brinkman number, $Br = \mu u_b^2/k(T_s - T_b)$, or $Br^* = \mu u_b^2/q_s b$, that are not negligibly small, indicating that viscous dissipation may play a role.

Section 5.2 of our heat transfer texts presents an analysis of Couette flow with viscous dissipation for a continuum model ($Kn \to 0$). Exercise 5.11 of these texts requires an analysis of flow in a circular tube with dissipation, also for a continuum model; Exercise 5.66 in H.T. considered flow between parallel plates. In addition, Supplement No. 2 on our website presents a detailed discussion of flow in channels with viscous dissipation, with an emphasis on the consequences of using various continuum flow models.

The role played by viscous dissipation in the Knudsen layer complicates the analysis of slip flows. Thus, although our main interest is channel flows, it is useful to analyze Couette flow with slip and viscous dissipation, to illuminate the evaluation of dissipation in the Knudsen layer.

2 COUETTE FLOW

The Couette flow model is described in Section 5.2.1 of our heat transfer texts. Two infinite parallel plates are spaced L apart: the plate at $y = 0$ is stationary while the plate at $y = L$ moves with a uniform velocity u_e. The plate at $y = 0$ is maintained at temperature T_s, and the plate at $y = L$ at T_e. (see Fig. 5.1 of our texts). Although not necessary, we will take $T_s > T_e$. The sketch shows the velocity profile for a slip velocity u_s. Equation 1 gives the slip velocity as

$$u_s = \alpha\lambda \frac{du}{dy}\Big|_s$$

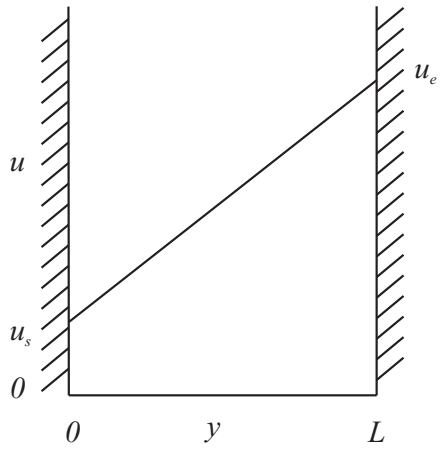

For the Couette flow the velocity profile is linear,

$$u = u_s + \frac{y}{L}(u_e - u_s) \tag{3}$$

Notice that we can specify the velocities u_s and $u_e - u_s$ at $y = 0, L$ because λ/L is very small. Then

$$u_s = \alpha\lambda\frac{u_e - 2u_s}{L} = \alpha Kn(u_e - 2u_s); \quad Kn = \frac{\lambda}{L}$$

Hence,

$$\frac{u_s}{u_e} = \frac{\alpha Kn}{1 + 2\alpha Kn} \tag{4}$$

The thermal energy equation is given by Eq. 5.5 in the texts,

$$k\frac{d^2T}{dy^2} + \mu\left(\frac{du}{dy}\right)^2 = 0 \tag{5}$$

The dissipation in the flow is

$$D = \int_0^L \mu\left(\frac{du}{dy}\right)^2 dy = \int_0^L \frac{\mu(u_e - 2u_s)^2}{L^2} dy = \frac{\mu(u_e - 2u_s)^2}{L} \tag{6}$$

The power input to sustain the flow is

$$P = u_e\mu\frac{du}{dy}\Big|_L = \mu\frac{u_e(u_e - 2u_s)}{L} \tag{7}$$

The dissipation at the walls is then

$$D_s = P - D = \frac{\mu}{L}[u_e(u_e - 2u_s) - (u_e - 2u_s)^2]$$
$$= \frac{\mu}{L}[2u_e u_s - 4u_s^2]$$
$$D_s = \frac{2\mu u_s(u_e - 2u_s)}{L} \tag{8}$$

At each wall the dissipation is

$$\frac{1}{2}D_s = \frac{\mu u_s(u_e - 2u_s)}{L} \tag{9}$$

which is the shear stress times the slip velocity, as expected.

2.1 Adiabatic Wall

We now consider the wall at $y = 0$ to be adiabatic, and the moving wall to be at temperature T_e, as for the continuum flow analyzed in Section 5.2. Integrating Eq. (5)

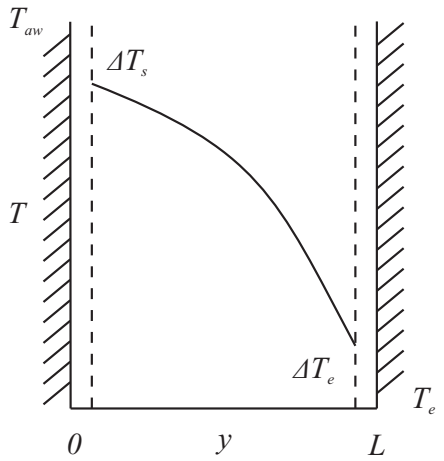

$$\frac{dT}{dy} = -\frac{\mu(u_e - 2u_s)^2}{kL^2}y + C_1$$

At $y = 0$ the heat flow is the wall dissipation. From Eq. (9),

$$-k\frac{dT}{dy}\Big|_0 = \frac{\mu u_s(u_e - 2u_s)}{L}$$

Hence

$$\frac{dT}{dy}\Big|_0 = -\frac{\mu u_s(u_e-2u_s)}{kL} = C_1$$

$$\frac{dT}{dy} = -\frac{\mu(u_e-2u_s)^2}{kL^2}y - \frac{\mu u_s(u_e-2u_s)}{kL} \tag{10}$$

Integrating again,

$$T = -\frac{1}{2}\beta\left(\frac{y}{L}\right)^2 - \zeta\frac{y}{L} + C_2 \text{ where } \beta = \frac{\mu(u_e-2u_s)^2}{k};\ \zeta = \frac{\mu u_s(u_e-2u_s)}{k}$$

$$y = L, \quad T + \Delta T_e = -\frac{1}{2}\beta - \zeta + C_2$$

$$C_2 = (T+\Delta T_e) + \frac{1}{2}\beta + \zeta$$

Hence,

$$T = \frac{1}{2}\beta\left(1-\frac{y^2}{L^2}\right) + \zeta\left(1-\frac{y}{L}\right) + (T_e + \Delta T_e) \tag{11}$$

where the temperature "jump" ΔT_e is taken as a positive quantity, i.e., $\Delta T_e = T_L - T_e$. Likewise the temperature jump $\Delta T_s = T_{aw} - T_0$ is taken as positive. Then

$$T_{aw} - T_e = \Delta T_s + \frac{1}{2}\beta + \zeta + \Delta T_e \tag{12}$$

Since $K_n = \lambda/L$ define a factor ϕ for Eq. (2) so that

$$\Delta T_s = \phi L\frac{dT}{dy}\Big|_0; \qquad \phi = \alpha_T\frac{2\gamma}{\gamma+1}\frac{Kn}{Pr}$$

$$\Delta T_s = \phi\zeta \tag{13}$$

and

$$\Delta T_e = \phi L\frac{dT}{dy}\Big|_L = \phi(\beta+\zeta) \tag{14}$$

Substituting in Eq. (12) gives our result,

$$T_{aw} - T_e = \phi\xi + \left(\frac{1}{2}\beta + \xi\right) + \phi(\beta+\xi) \tag{15}$$

where $\beta = \dfrac{\mu(u_e-2u_s)^2}{k}$; $\xi = \dfrac{\mu u_s(u_e-2u_s)}{k}$

$$\frac{u_s}{u_e} = \frac{\alpha Kn}{1+2\alpha Kn}; \quad \phi = \alpha_T\frac{2\gamma}{\gamma+1}\frac{Kn}{Pr}.$$

2.2 Sample Calculation for Knudsen number $= 0.15$.

Parameter values: $Kn = 0.15$, $\alpha = 1.11$, $\alpha_T = 1.13$, $Pr = 0.67$, $\gamma = 1.67$

$$\frac{u_s}{u_e} = \frac{(1.11)(0.15)}{1+(2)(1.11)(0.15)} = 0.125$$

$$\phi = (1.13)\frac{(2)(0.167)}{1+1.67}\frac{0.15}{0.67} = 0.317$$

Choose $\frac{\mu u_e^2}{2k} = 10\text{K}$, which is the continuum limit for $(T_{aw} - T_e)$.

$$\beta = 20[1-(2)(0.125)]^2 = 11.3; \quad \xi = (20)(0.125)[1-(2)(0.125)] = 1.88$$

$$\begin{aligned} T_{aw} - T_e &= (0.317)(1.88) + [(0.5)(11.3) + (1.88)] + (0.317)(11.3+1.88) \\ &= 0.596 + 7.50 + 4.15 \\ &= 12.2 \text{ K} \end{aligned}$$

2.3 Comparison with Continuum Flow

Power input:

continuum flow: $P_C = \frac{\mu u_e^2}{L}$

slip flow: $P_S = \frac{\mu u_e(u_e - 2u_s)}{L}$

$$\frac{P_S}{P_C} = \frac{u_e(u_e-2u_s)}{u_e^2} = \left(1 - 2\frac{u_s}{u_e}\right) = [1-(2)(0.125)] = 0.75$$

Flow dissipation:

continuum flow $D_C = \frac{\mu u_e^2}{L}$

slip flow $D_S = \frac{\mu(u_e-2u_s)^2}{L}$

$$\frac{D_S}{D_C} = \left(1 - 2\frac{u_s}{u_e}\right)^2 = (0.75)^2 = 0.563$$

From Eq. (8) the dissipation at the walls for slip flow is

$$D_{WS} = \frac{2\mu u_s(u_e - u_s)}{L}$$

$$\frac{D_{WS}}{D_C} = 2\left(\frac{u_s}{u_e}\right)\left(1 - 2\frac{u_s}{u_e}\right) = (2)(0.125)(0.75) = 0.182$$

and $(0.563 + 0.187) = 0.75 = P_S/P_C$, Also, $\frac{D_{WS}}{D_S} = \frac{0.187}{0.563} = 0.33$

In this slip flow, one third of the dissipation occurs at the walls. Notice that the larger temperature jump is at the moving plate,

$$\Delta T_s = \phi\gamma = (0.317)(1.67) = 0.53 \text{ K}$$

$$\Delta T_e = \phi(\gamma+\beta) = (0.317)(1.67+11.3) = 4.11 \text{ K}$$

The temperature jump ΔT_S is smaller because it only accounts for the wall dissipation flux.

3 CONCLUDING REMARKS

A number of papers dealing with flows in microchannels and microtubes have appeared recently, for example [1,2]. The objective of this supplement is to examine the role played by viscous dissipation in the Knudsen layer, and hence ensure a correct set of governing equations for the heat transfer problem.

REFERENCES

1. Colin, S., "Gas microflows in the slip flow regime: a critical review on convective heat transfer." ASME Journal of Heat Transfer, 134(2):020908–020908-13 (2011)

2. Asako, Y., and Hong, Chumpyo, "On temperature jump condition for slip flow in a microchannel with constant wall temperature." ASME Journal of Heat Transfer, 139(7): 072402–072402–7 (2017)

SUPPLEMENT

4

DISTRIBUTIONS OF MOLECULES AND PHOTONS

CONTENTS

1 Molecular Distributions 30
2 Photon Distributions 33

1 MOLECULAR DISTRIBUTIONS

In our HT and MT texts we wrote down the molecular flux without proof, citing the kinetic theory of gases (HT Eq. (7.103) which is then also used in Section 1.7 of MT). In order to derive these relations from first principles we need to introduce the concept of a molecular distribution. A monatomic molecule in a large container may have any velocity v (we exclude velocities approaching the speed of light), and at that velocity has momentum $p = \mathscr{m}v$ and energy $E = \frac{\mathscr{m}v^2}{2}$ (neglecting electronic excitation that occurs at high temperatures).

Consider an enclosure at thermodynamic equilibrium filled with a monatomic gas. The molecules are distributed on the average uniformly through the volume with a total number per unit volume of $P/\kappa_B T$. They are colliding randomly and, as a result on an average moving uniformly in all directions (that is, if a small volume of them were suddenly removed from the enclosure and placed at the center of a large sphere, and the molecules continued in motion without further collisions, the number eventually hitting the sphere per unit area would be uniform over the sphere.) The number of molecules $d\mathscr{N}$ whose energies lie between E and $E + dE$ is given by Maxwell-Boltzmann statistics as

$$d\mathscr{N} = \mathscr{N} \frac{2}{\pi^{1/2}} \left(\frac{E}{\kappa_B T} \right)^{1/2} \exp\left(-\frac{E}{\kappa_B T} \right) \frac{dE}{\kappa_B T} \tag{1}$$

A good text on statistical thermodynamics or statistical dynamics is recommended for those who would like to appreciate the foundation of Eq. (1); here we take the result on faith. In such texts Eq. (1) is used to derive many of the thermodynamic properties of gases (not too close to their critical points).

The number of molecules between two energies E_1 and E_2 can be found by integrating from E_1 to E_2 with respect to E. Changing variables from E to $E^* = E/\kappa_B T$ gives

$$\Delta\mathscr{N} = \mathscr{N} \frac{2}{\sqrt{\pi}} \int_{E_1^*}^{E_2^*} {E^*}^{1/2} \exp(-E^*) dE^* \tag{2}$$

The integration can be readily computed using, for example, Simpson's rule. However, one is more often interested in the number of molecules crossing a surface per unit time that have energies between E_1 and E_2 and the energy that they transfer.

Consider a surface dA in our enclosure at thermodynamic equilibrium. Molecules coming up through the surface in a particular direction have a velocity normal to the surface of $v\cos\theta$, where θ is the angle between the normal and the direction of interest. But how many molecules come from this direction? We imagine a sphere with its center at the centroid of our small surface dA, and mark off an area dA_s on the sphere. Then the question becomes, how many molecules come from dA in directions that cross the small area on the sphere dA_s?

The number of molecules crossing the surface dA per unit time in the energy range between E and $E + dE$ is $d\mathscr{N}$ times the normal component of the velocity v. Since the molecule trajectives are uniformly distributed in all directions, the fraction of these particles that cross dA_s is dA_s/A_s where A_s is the total area of our imagined sphere of radius r, $4\pi r^2$. Denoting the flux across the plane containing dA as $d\mathscr{J}^+$,

we have

$$d\mathscr{J}^+ = d\mathscr{N} v\cos\theta\left(\frac{dA_s}{A_s}\right) \tag{3}$$

The concept of a solid angle was introduced in section 6.5.1 of HT, BHT and BHMT. Since $d\omega = dA_s/r^2$ and $A_s = 4\pi r^2$,

$$\frac{dA_s}{A_s} = \frac{r^2 d\omega}{4\pi r^2} = \frac{d\omega}{4\pi}$$

Equation (3) then becomes

$$d\mathscr{J}^+ = d\mathscr{N} v\cos\theta\frac{d\omega}{4\pi} \tag{4}$$

To obtain the total number of molecules crossing per unit area in all directions and with all possible energies, we integrate over all directions in the hemisphere and over all possible energies from zero to infinity. Using polar coordinates, as shown in Figure 2,

$$d\omega = \frac{rd\theta r\sin\theta d\theta}{r^2} = \sin\theta d\theta d\phi \tag{5}$$

For the first integration

$$\int_{2\pi}\cos\theta d\omega = \int_0^{2\pi}\int_0^{\pi/2}\cos\theta\sin\theta d\theta d\phi = \pi \tag{6}$$

Thus we obtain the result after the first integration simply by replacing $\cos\theta d\omega$ in Eq. (4) with π,

$$d\mathscr{J}^+ = \frac{1}{4}vd\mathscr{N} = \frac{1}{4}v\frac{d\mathscr{N}}{dE}dE \tag{7}$$

Substituting Eq. (1), using $E = \frac{1}{2}\mathscr{m}v^2$ to express v as $(2E/\mathscr{m})^{1/2}$, and integrating with respect to E gives

$$\begin{aligned}\mathscr{J}^+ &= \int_0^\infty \frac{1}{4}\left(\frac{2E}{\mathscr{m}}\right)^{1/2}\mathscr{N}\frac{2}{\pi^{1/2}}\left(\frac{E}{\kappa_B T}\right)^{1/2}\exp\left(-\frac{E}{\kappa_B T}\right)\frac{dE}{\kappa_B T}\\ &= \frac{1}{4}\left(\frac{8\kappa_B T}{\pi\mathscr{m}}\right)^{1/2}\mathscr{N}\int_0^\infty E^* e^{-E^*}dE^* \text{ where } E^* = \frac{E}{\kappa_B T}\\ J^+ &= \frac{1}{4}\mathscr{N}\left(\frac{8\kappa_B T}{\pi\mathscr{m}}\right)^{1/2} = \frac{1}{4}\mathscr{N}\bar{v}\end{aligned} \tag{8}$$

which is Eq. 7.103 of HT. Thus we have a derivation from the very fundamental Maxwell-Boltzmann molecular velocity distribution.

To obtain the rate of energy transfer by a monatomic molecular flux we multiply the flux of molecules by the energy per molecule. From Eqs. (4) and (1)

$$dQ^+ = EdJ^+ = Ed\mathcal{N}v\cos\theta dA\frac{d\omega}{4\pi}$$

$$dq^+ = \frac{d\dot{Q}^+}{dA} = E\mathcal{N}\frac{2}{\pi^{1/2}}\left(\frac{E}{\kappa_B T}\right)^{1/2}\exp\left(-\frac{E}{\kappa_B T}\right)\frac{dE}{\kappa_B T}v\cos\theta\frac{d\omega}{4\pi}$$

Again we substitute the relation $(2E/m)^{1/2}$ for v and integrate over a hemisphere with respect to $d\omega$ and over all possible energies from zero to infinity

$$q^+ = \frac{1}{4\pi}\int_{2\pi}\cos\theta d\omega\frac{2v}{\pi^{1/2}}\int_0^\infty E\left(\frac{E}{\kappa_B T}\right)^{1/2}\left(\frac{2E}{m}\right)^{1/2}\exp\left(-\frac{E}{\kappa_B T}\right)\frac{dE_b}{\kappa_B T}$$

$$= \frac{1}{4}\left(\frac{8k_B T}{\pi m}\right)^{1/2}k_B T\mathcal{N}\int_0^\infty {E^*}^2 e^{-E^*}dE^*$$

$$= \frac{1}{4}\overline{v}\mathcal{N}(\kappa_B T)$$

$$q^+ = \mathcal{J}^+(2\kappa_B T) \qquad \textbf{(9)}$$

The average energy per molecule in the volume is not $2\kappa_B T$; it may be found by multiplying Eq. (5) by E and integrating with respect of E from zero to infinity. For a monatomic gas it is $\frac{3}{2}\kappa_B T$. However, the more energetic molecules in the volume are faster and cross an area dA more frequently. It is for this reason that the energy flux is the molecular flux multiplied by $2\kappa_B T$, rather than $\frac{3}{2}\kappa_B T$.

Polyatomic molecules carry energy also in their rotations and vibrations. The average internal energy of these molecules is mu, where u is the internal energy per unit mass. Of this total, the amount contained in the rotational and vibrational energies is on an average $mu - \frac{3}{2}\kappa_B T$, since the translational energy is on an average $\frac{3}{2}\kappa_B T$. If the vibrational-rotational energy is independent of the translational energy (a good approximation) then the rate of energy transfer crossing a plane (in one direction) in a polyatomic gas is

$$q^+ = \mathcal{J}^+(mu + \frac{1}{2}\kappa_B T) \qquad \textbf{(10)}$$

A complicating factor is the fact that during a molecule-surface collision, the vibrational energies are usually transferred much less efficiently than are the translational and rotational energies. There is a probabilistic nature to molecule-surface interaction. Some impinging molecules "stick" to the surface in an adsorbed layer for a rather long time, during which time their energies are *accommodated* to the distribution characteristic of the surface temperature. Other stick not at all or only briefly so that little energy is transferred. Usually a high fraction, say 90% of the incident molecules stick long enough to many types or dirty engineering surfaces to give up their translational and rotational energies and acquire those characteristic of the surface. Note also that many molecules are vibrationally unexcited at nor-

mal temperatures; thus this complication does not affect transport in those cases. Of course, perfect accommodation would correspond to a "black" surface.

An issue that might confuse the student are the terms $2\kappa_B T$ in Eq. (9), and the $1/2\kappa_B T$ in Eq. (10) for a monatomic gas. In constrast, Eq. (2.219) of MT gives the interdiffusion energy flux in a monatomic gas as

$$q_{id} = \frac{5}{2}\kappa_B T \sum_{i=1}^{n} \mathscr{N}_i \hat{v}_i \tag{11}$$

So why is this "energy" flux different to those given by Eqs. (9) and (10)? The answer is that Eq. (11) gives an *enthalpy* flux associated with the diffusion fluxes of the various species.

This point can be illuminated by examining the derivation of the energy equation using a continuum formulation, as was done for the laminar boundary layer on a flat plate in Section 2.5.2 of MT use of the steady flow energy equation, which includes work effects, gives the heat flux in Eqs. (2.158) and (2.159) as

$$q = -k\frac{\partial T}{\partial y} + \sum j_{i,y} h_i \tag{12}$$

Since $c_p = c_v + \frac{\mathscr{R}}{M}$, $c_p = c_v + \frac{\kappa_B}{\mu}$, and for a monatomic gas $c_v = \frac{3}{2}\kappa_B T$,

$$dh_i = c_{pi} dT = \left(\frac{3}{2} + 1\right)\kappa_B T = \frac{5}{2}\kappa_B T \tag{13}$$

2 PHOTON DISTRIBUTIONS

Following Section 1, now consider a black enclosure at thermodynamic equilibrium filled with photons. The energy distribution is given by a limit form of Bose-Einstein statistics: the number of photons per unit volume $d\mathscr{N}$ whose energies lie between E and $E + dE$ is

$$d\mathscr{N} = \frac{8\pi}{(\hbar c/\kappa_B T)^3} \frac{(E/\kappa_B T)^2}{\exp(E/\kappa_B T) - 1} \frac{dE}{\kappa_B T} \tag{14}$$

and may be termed the Planckian or blackbody distribution.

Again consider a surface dA with the angle θ being the zenith angle between the normal z-direction and a generic vector r in polar coordinates. In a standard polar coordinate system, the angle ϕ is the azimuth angle, which is counted as positive from the x-axis to the projection of the r-vector onto the $x - y$ plane that contains dA. Denoting the photon flux across the plane containing dA as $\dot{\mathscr{N}}$ we have an analogy to Eq. (3) for molecules,

$$d\dot{\mathscr{N}} = d\mathscr{N} c \cos\theta dA \frac{d\omega}{4\pi} \tag{15}$$

To obtain the energy flux (*power*) crossing dA we multiply $d\dot{\mathcal{N}}$ by the energy carried by each photon,

$$d\dot{Q} = E\,d\dot{\mathcal{N}}$$

$$d\dot{Q} = (\hbar c\nu)(d\mathcal{N}\, c\cos\theta \frac{d\omega}{4\pi}) \tag{16}$$

where $d\mathcal{N}$ is given by Eq. (14). The concept of radiation intensity was introduced as Eq. (6.57) of our heat transfer texts. Here we define a Planckian (blackbody) spectral radiation intensity that is independent of directions θ and ϕ.

$$I_{b\nu} = \frac{d\dot{Q}}{(dA\cos\theta)d\omega d\nu} \tag{17}$$

Substituting Eqs. (14) and (16) gives

$$I_{b\nu} = \frac{2\hbar c^2\nu^3}{\exp(\hbar c\nu/\kappa_B T) - 1} \tag{18}$$

To obtain the total energy flux crossing dA in all directions to the hemisphere above it, and for photons of all possible wavenumbers from zero to infinity, we integrate Eq. (17) over $d\omega$ and $d\nu$. We have already done the integration over $d\omega$ in deriving Eq. (6.60) of our texts

$$E_{b\nu} = \frac{d\dot{Q}}{dA\; d\omega} = \pi I_{b\nu} \tag{19}$$

The quantity $E_{b\nu}$ is the energy flux crossing dA whose photon wavenumbers lie between ν and $\nu + d\nu$, and is the spectral or *monochromatic emissive power* introduced in Eq. (6.5) of our texts.

Next we integrate $E_{b\nu}$ over all possible wavenumbers from zero to infinity. The integral is well behaved because the probability of zero wavenumber photons is zero, from Eq. (14) like $2\kappa_B T c\nu^2$ in the limit, and for infinite wavenumbers is also zero, like $2\hbar c\, \nu^3 \exp(-\hbar c\nu/\kappa_B T)$.

$$E_b(T) = \int_0^\infty \pi I_{b\nu} d\nu$$

Substituting Eq. (22),

$$E_b(T) = \int_0^\infty \frac{2\pi\hbar c^2\nu^3}{\exp(\hbar c\nu/\kappa_B T) - 1} d\nu$$

Changing variables from ν to $\hbar c\nu/\kappa_B T$ yields

$$E_b(T) = \frac{2\pi\kappa_B^4 T^4}{\hbar^3 c^2} \int_0^\infty \frac{\zeta^3 d\zeta}{\exp\zeta - 1}$$

The definite integral has a value of $\pi^4/15$; therefore

$$E_b(T) = \frac{2\pi^5\kappa_B^4}{15\hbar^3 c^2} T^4 \tag{20}$$

The coefficient multiplying T^4 is the Stefan–Boltzmann constant σ,

$$\sigma = \frac{2\pi^5 \kappa_B^4}{15\hbar^3 c^2} = 5.6697 \times 10^{-8} \text{ W/m}^2\text{K} \tag{21}$$

Exercise 6.3 of Chapter 6 requires a derivation of the Stefan–Boltzmann constant using Planck's law as given by Eq. (6.5). In Eq. (6.5) the spectral variable is wavelength whereas in Eq. (18) it is wavenumber $v = 1/\lambda$. Substituting for C_1 and C_2 in Eq. (6.5) using the values given in the relevant footnote,

$$E_{b\lambda} = \frac{dE_b}{d\lambda} = \frac{2\pi\hbar c^2 \lambda^{-5}}{\exp(\hbar c/\kappa_B T) - 1}$$

Now $\frac{dE_b}{dv} = \frac{dE_b}{d\lambda} \cdot \frac{d\lambda}{dv}$ and $\frac{d\lambda}{dv} = \frac{d}{dv}\left(\frac{1}{v}\right) = -\frac{1}{v^2} dv$ where the minus sign can be ignored since it simply indicates that wavelength decreases as wavenumber increases. Then

$$E_{bv} = \frac{dE_b}{dv} = \frac{2\pi\hbar c^2 v^3}{\exp(\hbar cv/\kappa_B T) - 1} = \pi I_{bN}$$

which is equivalent to Eq. (6).

In Section 2 we have shown how Planck's law and the Stefan–Boltzmann law follow from the Planckian limit of Bose–Einstein statistics which gave the number of photons per unit volume $d\mathcal{N}$ in a black enclosure in thermodynamic equilibrium, whose energies lie between E and dE.

As for Equation (1) which gave the Maxwell–Boltzmann distribution, a good text on statistical thermodynamics is recommended to obtain an understanding of the origins of Eq. (14).

Acknowledgement

The material in this note originally appeared in the text "Transport Processes" by D.K. Edwards, V.E. Denny and A.F. Mills (Holt, Rinehart and Winston, 1973), wherein Chapter 6 was contributed by the late Professor D.K. Edwards.

SUPPLEMENT

5

FREE MOLECULE CONDUCTION

CONTENTS

1 Introduction 38
2 Molecular Fluxes 38
3 Transport Between Infinite Parallel Black Walls 40

1 INTRODUCTION

In BHMT and MT we encountered *Knudsen diffusion* in dealing with diffusion in porous catalysis when the pressure was low or the pores very small. Then molecules collided with the pore walls more frequently then with each other, and the motion of molecules along a pore was governed by the equations for *free molecule flow*. The *Knudsen number* Kn is defined as the ratio of the mean free path of the gas molecules to a characteristic length scale: for a pore this scale is the pore radius or diameter. Similarly, for heat conduction in a gas in a geometry for which the Knudsen number is large, Fourier's law is not valid and instead we have *free molecule conduction*.

The physics of free molecule transport is analogous to the physics of photon transport and hence radiation heat transfer. In both cases the mean free path of the energy carrier is long compared to the characteristic length scale of relevance. Also, the concept of a *black* surface is analogous for both phenomena. For a monatomic gas the molecular energy distribution is given by *Maxwell-Boltmann* statistics, whereas for photons the photon energy distribution is given by *Bose-Einstein* statistics. Many surfaces encountered in technology can be idealized as being black to photons and/or molecules. The term *black* merely denotes that no photons or molecules are reflected from the surface: all photons are *absorbed* and all molecules are either *adsorbed* or *condense*. Whether or not a surface is black or nearly so can be determined, for example, by directing a stream of molecules from a source in a vacuum chamber onto a surface and determining whether or not they are promptly reflected with the same energies they possessed before striking the surface. Much the same can be done with photons from a radiant source. An obvious consequence of our definition of a black surface is that all photons, or molecules, leaving the surface are *emitted* by the surface.

In Section 2, expressions for the molecular flux and energy flux impinging on a surface will be written down without proof. However, derivations using the Maxwell-Boltmann distribution of molecular energies are given in Supplement No. 4.

2 MOLECULAR FLUXES

The molecular flux bombarding a surface is denoted as $\mathscr{J}^-$ molecules/m^{2}s. When a gas is in thermodynamic equilibrium the kinetic theory of gases shows that

$$\mathscr{J}^- = \frac{1}{4}\mathscr{N}\overline{v} \tag{1}$$

where $\mathscr{N}$ is the number of molecules per unit volume given by the ideal gas law, and $\overline{v}$ (also denoted c) is the average molecular speed,

$$\mathscr{N} = \frac{P}{\kappa_B T} \quad \overline{v} = \left(\frac{8\kappa_B T}{\pi m}\right)^{1/2} \tag{2a,b}$$

Boltzmann's constant κ_B is the gas constant per molecule, that is, the universal gas constant divided by Avogadro's number. The molecular mass M is obtained by multiplying the atomic mass unit, $u = 1.6605 \times 10^{-27}$ kg, by the molecular weight.

Now consider a gas contained in an enclosure, the walls of which are coated with the condensed phase of the gas – imagine water vapor with the walls coated by liquid water or ice, the surface of which will be assumed to be black. At thermodynamic equilibrium the system is isothermal, and molecules must leave the walls at the same rate as which they arrive. The flux of molecules emitted by the condensed phase is then

$$\mathscr{J}_b^+ = \frac{1}{4}\mathscr{N}\overline{v} \tag{3}$$

where the subscript b denotes a black surface. Observe that Eq. (3) has thus been derived from thermodynamics: no physical model for the emission process has been postulated. Notice also that Eq. (3) is the molecular analog of the Stefan-Boltzmann law, Eq. (6.7) of HT or BHMT, and too can be regarded for now as a physical law based on experiment. As was the case for photons, experiments on the evaporation or various substances into a vacuum have shown the law to be valid, that is, even when the incident flux is zero.

The flux of energy striking a black surface being bombarded by molecules is obtained by multiplying the flux of molecules by the energy they bring to the surface. In deriving Eq. (1.104) of MT we observed that, on an average, each molecule has a kinetic energy of $(3/2)\kappa_B T$; however, the more energetic molecules arrive more frequently so that the energy transport per molecule proves to be $2\kappa_B T$. Thus

$$q^- = \frac{1}{4}\mathscr{N}\overline{v}(2\kappa_B T) \tag{4}$$

for a monatomic gas. A polyatomic gas carries additional energy so we can write more generally

$$q^- = \frac{1}{4}\mathscr{N}\overline{v}\left(\mathscr{m}u + \frac{1}{2}\kappa_B T\right) \tag{5}$$

where u is the internal energy per unit mass.

In Supplement 4 we will provide rigorous derivations of Eqs. (3) and (4) after we have introduced the Maxwell-Boltzmann distribution of molecular energies.

EXAMPLE 5.1 Evaporation of Aluminum into a Vacuum

An aluminum surface at 889°C is exposed to a vacuum. Determine the rate of evaporation. The *Handbook of Chemistry and Physics* gives the saturation vapor pressure of aluminum at 889°C as 1.00×10^{-3} torr.

Solution

Given: Aluminum surface at 889°C in a vacuum.

Required: Evaporation rate

Assumptions: 1. The surface is black for molecules.

The saturation vapor pressure is precisely the pressure of pure vapor which would be in equilibrium with the condensed phase at the specified temperature. Therefore we can use Eq.

(3) directly.

$$\mathscr{J}_b^+ = \frac{1}{4}\mathscr{N}\overline{v}$$

Assuming monatomic vapor ($M = 27.0$) we obtain

$$\overline{v} = \left(\frac{8\kappa_B T}{\pi m}\right)^{1/2} = \left[\frac{(8)(1.381\times10^{-23})(1162)}{(\pi)(1.660\times10^{-27})(27.0)}\right] = 955 \text{ m/s}$$

The molar concentration is

$$c = \frac{P}{\mathscr{R}T} = \frac{(10^{-3}/760)(1.013\times10^5)}{(8314)(1162)} = 1.380\times10^{-8}\,\text{kmol/m}^3$$

$$\mathscr{N} = c\mathscr{A} = (1.380\times10^{-8})(6.0221\times10^{26}) = 8.310\times10^{18}\text{molecules/m}^3$$

$$\mathscr{J}_b^+ = (1/4)(8.310\times10^{18})(955) = 1.984\times10^{21}\text{ molecules/m}^2\text{s}$$

On a mass basis,

$$n = (1.984\times10^{21})(27)/(6.0221\times10^{26}) = 8.90\times10^{-5}\text{ kg/m}^2\text{s}$$

3 TRANSPORT BETWEEN INFINITE PARALLEL BLACK WALLS

Recall that thermal radiation (photon transport) between infinite parallel surfaces, 1 and 2, is given by simple relation

$$q_{12} = \sigma T_1^4 - \sigma T_2^4 \tag{6}$$

Exactly the same can be written for two parallel walls exchanging mass. The net flux is simply

$$\frac{1}{4}\mathscr{N}_1\overline{v}_1 - \frac{1}{4}\mathscr{N}_2\overline{v}_2 = \mathscr{J}^+ - \mathscr{J}^- \tag{7}$$

where $\mathscr{N}_1$ is calculated using the saturation vapor pressure at surface temperature T_1 of the one wall, and $\mathscr{N}_2$ is similarly calculated for the second surface. But Eq. (7) is not particularly useful. For example, it describes transfer of mass across the gap between the walls when both walls are of the same substance: the one at the higher temperature undergoes net evaporation, and the other net condensation. Such a situation is not of much practical importance.

The more usual engineering situation is of two parallel walls containing a superheated gas with no net transfer of gas. Suppose that the pressure is low enough for the distance between the walls to be small compared to the mean free path so that "free molecule" conduction will take place. The left wall is at temperature T_1, and the right one is colder at T_2. The surfaces are black to incident molecules (though not necessarily to photons). Then the molecules are adsorbed on the walls long enough for those that are reemitted to have the statistical nature of a gas in thermal equilibrium with the wall.

The situation described above occurs quite commonly in the vacuum jackets around tubes and containers used to hold cryogenic liquids, such as liquid hydrogen,

natural gas and nitrogen. An evacuated space around the container is used to reduce the boil-off losses of these cryogens. Evacuation reduces the number density so that there are few energy carriers, and an assembly of shields with spacing less than the mean free path is used to prevent molecules (and photons) from crossing directly to the cold inner wall in contact with the cryogen from the relatively hot outer wall at the temperature of the surroundings.

Once one wall is heated and the other cooled to give a steady state, the molecules in each space divides itself into two populations, one consisting of molecules going from left to right at number density $\mathscr{N}_1^+$, and one going from right to left, $\mathscr{N}_2^-$. The sum of the two equals the whole population,

$$\mathscr{N} = \mathscr{N}_1^+ + \mathscr{N}_2^- \tag{8}$$

We assume that the wall material has a very low vapor pressure so molecules of the wall material are not subliming from one wall and condensing on the other. Then at steady state the flux of molecules going from left to right $\mathscr{J}^+$ equals the flux from right to left, $\mathscr{J}^-$

$$\mathscr{J}^- = \mathscr{J}^+ \tag{9}$$

In Eqs (1, 3) the quantity $\mathscr{N}$ was the total population. However, when T_1 equals T_2, the quantity $\mathscr{N}$ was twice the population $\mathscr{N}_1^+$ of the molecules going one way. Thus Eqs. (1, 2a,b) may be rewritten generally as

$$\mathscr{J}^- = \frac{1}{2}\mathscr{N}_2^- \overline{v}_2 \tag{10a}$$

$$\mathscr{J}^+ = \frac{1}{2}\mathscr{N}_1^+ \overline{v}_1 \tag{10b}$$

Because the surface are black, the emitted molecules from each have a velocity distribution that characterises equilibrium emission. Therefore

$$\overline{v}_1 = \left(\frac{8\kappa_B T_1}{\pi m}\right)^{1/2}; \quad \overline{v}_2 = \left(\frac{8\kappa_B T_2}{\pi m}\right)^{1/2} \tag{11a,b}$$

Equations (8) to (10b) are a set of four algebraic equations in four unknowns that must be solved. Substituting Eqs. (10a) and (10b) into (9) using (8) to eliminate $\mathscr{N}_2^-$ gives

$$\mathscr{N}_1^+ = \mathscr{N}\frac{\bar{v}_2}{\overline{v}_1 + \bar{v}_2} = \mathscr{N}\frac{T_2^{1/2}}{T_1^{1/2} + T_2^{1/2}} \tag{12}$$

Equation (10b) then gives

$$\mathscr{J}^+ = \frac{1}{4}\mathscr{N}\left(\frac{8\kappa_B T_M}{\pi m}\right)^{1/2}; \quad T_M^{1/2} = \frac{2T_1^{1/2}T_2^{1/2}}{T_1^{1/2} + T_2^{1/2}} \tag{13}$$

The net energy flux is then the flux crossing from left to right minus that crossing from right to left. From Eq. (5), assuming c_V constant, we obtain

$$q_{\text{net}} = \mathscr{J}^+(mc_vT_1 + \frac{1}{2}\kappa_B T_1) - \mathscr{J}^-(mc_vT_2 + \frac{1}{2}\kappa_B T_2)$$

$$= \frac{1}{4}\mathscr{N}\left(\frac{8\kappa_B T_m}{\pi m}\right)^{1/2}(mc_v + \frac{1}{2}\kappa_B)(T_1 - T_2)$$

Introducing the ratio of specific heat γ and the relation $c_p = c_v + \kappa_B/m$ we obtain

$$q_{\text{net}} = \frac{1}{4}\mathscr{N}\left(\frac{8\kappa_B T_M}{\pi m}\right)^{1/2}\left(\frac{\gamma+1}{2\gamma}mc_p\right)(T_1 - T_2) \qquad \textbf{(14)}$$

This result gives the rate of heat transfer per unit area between two parallel plates when there is no net mass transfer. Note that $\kappa_B/m = \mathscr{R}/M$ and $\mathscr{N}m$ is the density ρ.

EXAMPLE 5.2 Superinsulation

A layer of multilayer insulation used to insulate LNG (liquid natural gas) has a gap width of 2.5mm, and is evacuated to 10^{-5} torr. Calculate the free molecule conduction heat flux across the gap when two adjoining surfaces are at 117K and 114K respectively. Compare this result to continuum conduction, and to radiation heat transfer if the layers are made from du Pont Mylar with vacuum deposited aluminum surfaces ($\varepsilon = 0.02$).

Solution

Given: Superinsulation with Mylar sheets, coated by vacuum deposited aluminum, 2.5mm apart.

Required: Heat transfer when two sheets are at 117 and 114K, respectively and the pressure is 10^{-5} torr (10^{-5} mm Hg)

Assumptions: 1. Surfaces black to molecules
2. Surface emittance for photons 0.02
3. Aluminum vapor pressure negligible

First calculate $\overline{v}$ for $T_M = 115.5$K.

$$\overline{v} = \left(\frac{8\kappa_B T_M}{\pi m}\right)^{1/2} = \left(\frac{(8)(1.381\times10^{-23})(115.5)}{(\pi)(1.660\times10^{-27})(29.0)}\right)^{1/2} = 289\,\text{m/s}$$

$$\rho = \frac{PM}{\mathscr{R}T_M} = \frac{(10^{-5})(1.013\times10^5)(29.0)}{(760)(8314)(115.5)} = 4.025\times10^{-8}\,\text{kg/m}^s$$

For air $c_p = 1005$ J/kg K and $\gamma = 1.4$. Substituting in Eq. (14),

$$q_{\text{cond}} = (1/4)(4.025\times10^{-8})(289)(2.4/2.8)(1005)(117-114) = 7.51\times10^{-3}\,\text{W/m}^2$$

If the mean free path were short compared to the gap width, continuum conduction would be

$$q = \frac{k\Delta T}{L} = \frac{(0.013)(117-114)}{2.5\times10^{-3}} = 15.6\,\text{W/m}^2$$

so that the evacuation to 10^{-5} torr reduces conduction by a factor of 2000.

The radiation heat transfer can be calculated from Eq. (6.41) of HT or BHMT.

$$q_{\text{rad}} = \frac{\sigma T_1^4 - \sigma T_2^4}{1/\varepsilon_1 + 1/\varepsilon_2 - 1}$$

Linearizing, $\sigma T_1^4 - \sigma T_2^4 = 4\sigma T_M^3 \, \Delta T$

$$q_{\text{rad}} = \frac{(4)(5.67 \times 10^{-8})(115.5)^3(3)}{1/0.02 + 1/0.02 - 1} = 1.06 \times 10^{-2} \, \text{W/m}^2$$

The total heat flux is

$$q_{\text{total}} = q_{\text{cond}} + q_{\text{rad}} = 7.51 \times 10^{-3} + 1.06 \times 10^{-2} = 1.81 \times 10^{-2} \text{W/m}^2$$

and $q_{\text{cond}}/q_{\text{rad}} = 7.51 \times 10^{-3}/1.06 \times 10^{-2} = 0.71$.

Comments

1. At this temperature the free molecule conduction remains at 42% of the total heat transfer. In some applications, evacuations to 10^{-7} torr are used to eliminate free molecule conduction.
2. The ratio of $q_{\text{cond}}/q_{\text{rad}}$ depends strongly on temperature level. The emittance of aluminum at these temperatures is approximately proportional to $T^{1/2}$. Check that $q_{\text{cond}}/q_{\text{rad}} \propto T^{-4}$. If the layer were at room temperature with $T_M = 294\text{K}$, $q_{\text{cond}}/q_{\text{rad}} = 0.0169$ and free molecule conduction is negligible compared to radiation heat transfer.

Acknowledgement

The material in this note originally appeared in the text "Transfer Processes" by D.K. Edwards, V.E. Denny and A.F. Mills (Holt, Rinehart and Winston, 1973). The relevant chapter, Chapter 6, was written by the late Professor D.K. Edwards.

SUPPLEMENT

6

DIMENSIONAL ANALYSIS OF PIPE FLOW

Experimental data for physical phenomena, as well as the results of analysis, can be conveniently and concisely organized as relationships between dimensionless groups of the pertinent variables. The simplest method for selecting dimensionless groups appropriate to a given problem is dimensional analysis using the Buckingham pi theorem and the method of indices. The methodology is presented in standard fluid mechanics texts; it is also given in Section 4.2.2 of our heat transfer texts, and it will be presumed that the student is familiar with the procedures. Our purpose here is to show how dimensional analysis should be used to obtain the dimensionless groups pertinent to pipe flow, and so correlate experimental data in a convenient form.

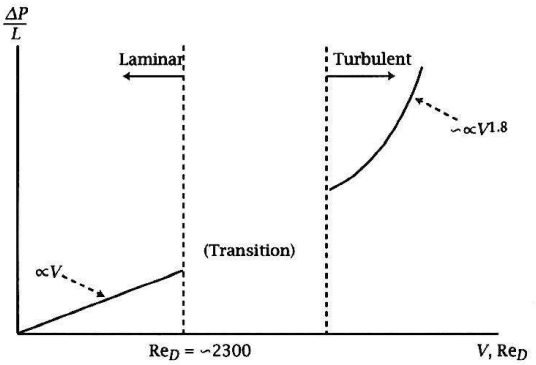

Figure 6.1: Pressure gradient as a function of velocity in pipe flow.

Engineers need to be able to calculate pressure drop for flow in a pipe in order to size pumps and fans to give the desired flow rate. For laminar flow an appropriate formula can be obtained by analysis, but for turbulent flow we must rely on experimental data. In a typical experiment, pressure drop data for turbulent flow are obtained as a function of flow rate for various pipe diameters. How should this data be presented in a form useful to an engineer? We will proceed by first considering the simpler case of laminar flow. To apply dimensional analysis we postulate that the pressure drop ΔP over a pipe length L depends on bulk velocity V, pipe diameter D, and viscosity μ, that is

$$\frac{\Delta P}{L} = \text{func}(V, D, \mu). \tag{1}$$

Notice we do not include density ρ because there are no inertia effects involved: the flow is neither accelerating nor decelerating. Application of the Buckingham pi theorem shows that there is only one possible dimensionless group,

$$\Pi_1 = \frac{D^2(\Delta P)/L}{\mu V} \tag{2}$$

and consequently it is a constant. In principle we need a single experimental data point to obtain the value of the constant, which proves to be 32. In fact, the analysis of laminar flow in a circular pipe, called *Pousielle flow*, is straightforward and is given in our texts Section 5.3.1, and confirms that $\Pi_1 = 32$. The product Π_1 is called

the Pousielle number Po, then

$$\frac{\Delta P}{L} = Po\frac{\mu V}{D^2}. \tag{3}$$

Now consider fully established turbulent flow for which the Reynolds number is greater than about 10,000, and look at data for $\Delta P/L$ as a function of velocity V, as shown in Fig. 6.1. We see that the increase in $\Delta P/L$ with velocity is not linear as for laminar flow, but increases more rapidly. The reason is that, in addition to molecular scale viscous stresses characterized by Newton's law of viscosity, there are shear stresses due to turbulent eddies moving transverse to the flow and exchanging momentum with the slower or faster moving fluid encountered, as shown in Fig. 6.2. The rate at which the eddies can transfer momentum is proportional to their mass, and hence to the fluid density ρ. So we need to perform a new dimensional analysis that includes ρ. We postulate

$$\frac{\Delta P}{L} = \text{func}(V, D, \mu, \rho) \tag{4}$$

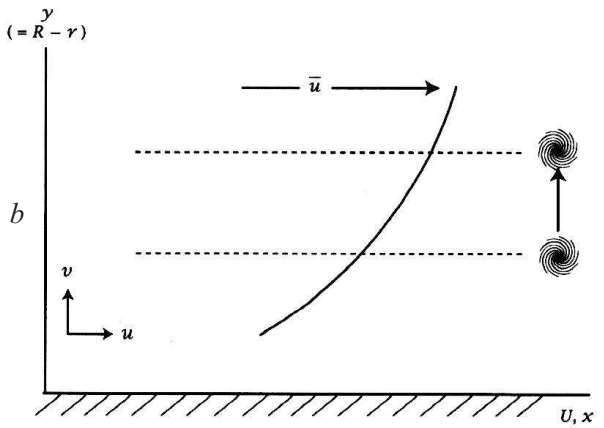

Figure 6.2: Momentum transfer by a turbulent eddy. An eddy that moves as shown will cause fluctuations in the instantaneous velocity components at b. Writing the instantaneous velocity as a sum of a time mean value and a fluctuating component, e.g. $u = \overline{u} + u'$ at b, u' will be negative and v' will be positive. In fact, the fluctuating components will always have opposite signs in a shear flow, and $\overline{u'v'}$ will always be nonzero. The turbulent shear stress is shown to equal $\overline{\rho u'v'}$ in fluid mechanics texts.

The Buckingham Pi-theorem now shows that there are two independent groups. We have already deduced Π_1 as a group; a second independent group is found to be

$$\Pi_2 = \frac{\rho V D}{\mu} \tag{5}$$

which is the familiar Reynolds number Re_D. Recall that these dimensionless groups are not unique; in particular, we can replace Π_1 by the quotient $\Pi_1/\Pi_2 = \Pi_3$,

$$\Pi_3 = \frac{D(\Delta P/L)}{\rho V^2} \tag{6}$$

and

$$\Pi_3 = \text{func } \Pi_2. \tag{7}$$

Let us denote $\Pi_3 = f$ a "friction factor", then

$$f = \text{func } Re_D \tag{8}$$

and

$$\frac{\Delta P}{L} = f\frac{\rho V^2}{D} \tag{9}$$

Now let us look at the physical significance of Po and f. Equation 2 can be rearranged as

$$Po = \frac{\Delta P(\pi D^2/4)}{\mu(V/4D)\pi DL} \tag{10}$$

or,

$$\Delta P\frac{\pi D^2}{4} = Po\mu\frac{V}{4D}\pi DL \tag{11}$$

which expresses the balance of the pressure force and wall shear force over a length L. Thus $Po\mu V/4D$ is the wall shear stress,

$$\tau_s = \frac{1}{4}Po\mu\frac{V}{D} = \mu\frac{\partial u}{\partial r}|_R \tag{12}$$

using Newton's law of viscosity. We should expect the velocity gradient at the wall to increase with bulk velocity V and decrease with diameter D: we say that the velocity gradient *scales* with V/D. In fact it is exactly proportional to V/D since Po is a constant. From Pouseille flow analysis, the velocity gradient is $8V/D$. We conclude that Po can be viewed as characterizing the ratio of pressure force to the wall shear force.

Similarly, for turbulent flow Eq. (9) can be rearranged as

$$\Delta P\frac{\pi D^2}{4} = \frac{1}{4}f\rho V^2\pi DL \tag{13}$$

or

$$f = \frac{\Delta P(\pi D^2/4)}{(1/4)\rho V^2\pi DL}. \tag{14}$$

Again, the wall shear stress from Eq. (13) is

$$\tau_s = \frac{1}{4} f \rho V^2 \tag{15}$$

and we see now that τ_s scales with ρV^2. It is not directly proportional to ρV^2; Eq. (14) states that f is a function of Reynolds number. Experiment shows it is a weak function (approximately proportional to $\mathrm{Re}_D^{-0.2}$).

It is relatively easy to see that the wall shear should scale with $\mu V/D$ in laminar flow; why it should scale with ρV^2 in turbulent flow is more difficult to explain to the beginning student. However, in most second courses in fluid mechanics it is shown that in turbulent flows we can write a velocity component as a sum of a mean value and a fluctuating component. Referring to Fig. 6.2,

$$u = \overline{u} + u' \tag{16a}$$

$$v = \overline{v} + v' \tag{16b}$$

and the turbulent shear stress is found to be $\overline{\rho u' v'}$. Since u' and v' must each scale with the bulk velocity V, the scaling ρV^2 of the shear stress results. It is important for the student to appreciate that the denominator of Eq. (14) scales the turbulent shear stress.

It has been standard practice of engineers for nearly a century to use the Darcy-Weisbach friction factor f to characterize pressure drop in pipe flow,

$$f = \frac{\Delta P/L}{\frac{1}{2}\rho V^2/D}. \tag{17}$$

Standard texts are not in agreement as to the physical significance of the denominator: some refer to the $\frac{1}{2}\rho V^2$ as the dynamic pressure of the flow, some say it is the kinetic energy of the flow, but both are inappropriate. First, the mean flow is steady so there are no inertia effects associated with the mean flow—the physics involves a balance of pressure and shear forces and dynamic pressure is irrelevant. Second, pressure drop is determined by Newton's laws of motion which reduce to this force balance—the kinetic energy of the mean flow is not involved and indeed does not change along the pipe. It is the 1/2 factor introduced in Eq. 17 by Weisbach that has confused matters. Of course he was free to include any numerical factor in his definition of friction factor, but his choice of 1/2 was unfortunate since it misled people as to the physical significance of the denominator. We have seen that the denominator scales the turbulent shear stress, and has nothing to do with dynamic pressure or kinetic energy.

In the case of turbulent flow there is no need to change the well-established practice of using the Darcy friction factor—the factor of 1/2 is included in the correlation of experimental data. A simple power law correlation is

$$f = 0.0184 \mathrm{Re}_D^{-0.5};\ 4 \times 10^4 < \mathrm{Re}_D < 10^6. \tag{18}$$

Alternatives include the more accurate Colebrook–White and Petukhov formulas. However, for laminar flow the use of the Darcy friction factor is really inappropriate

for another reason. For laminar flow, Pousielle flow analysis gives

$$f = \frac{64}{\mathrm{Re}_D} \tag{19}$$

and is shown, for example, on the Moody friction factor chart, Eq. (4.49) of our texts.

Equation (19) is easy enough to use but is also misleading since it falsely suggests that laminar flow depends on Reynolds number, and hence on density since $\mathrm{Re}_D = \rho VD/\mu$. If we combine Eq. (19) with Eq. (17),

$$\frac{\Delta P}{L} = 32\frac{\mu V}{D} \tag{20}$$

and it is clear that pressure drop depends neither on Reynolds number or density. Our dimensional analysis of laminar flow where the parameter ρ was not included at the outset yielded the correct result, namely Eq. (3)

$$\frac{\Delta P}{L} = Po\frac{\mu V}{D}; \quad Po = 32. \tag{21}$$

An added advantage of using Eq. (3) is that it is then simpler to show an analogy between momentum, heat and mass transfer in laminar pipe flow (Exercise 5–19).

Finally, let us discuss briefly the effect of wall roughness in turbulent flow. The Moody chart shows that there is a "fully rough" regime at high Reynolds numbers for which the Darcy friction factor is constant, i.e., is independent of Reynolds number and hence viscosity. Even in turbulent flow, on a smooth wall momentum must be transferred across a laminar sublayer in which turbulence is damped out and Newton's law of viscosity applies. But on a fully rough wall, momentum is transferred to the wall by *form drag* on the protruding roughness elements (the pressure on the front of such an element is higher than on the back due to flow separation). The shear stress due to viscosity is negligible by comparison. Form drag on a bluff body also scales with ρV^2, but now it is an inertia effect associated with velocity changes in the vicinity of the roughness elements. If viscosity is unimportant,

$$\frac{\Delta P}{L} = \mathrm{func}(V, D, \rho, \varepsilon) \tag{22}$$

where ε is a characteristic roughness height. Application of the Buckingham theorem then gives

$$\frac{\Delta P/L}{\rho V^2/D} = \mathrm{func}\left(\frac{\varepsilon}{D}\right) \tag{23}$$

and the Moody chart shows how the Darcy friction factor depends on ε_s/D, where ε_s is the *equivalent sandgrain roughness*, which is the size of close-packed sandgrains that gives the same friction factor as actual roughness pattern in the fully rough regime. Table 4.8 gives a formula for ε_s applicable to repeated rib roughness based on data obtained by previous experimenters. Section 4.7 discusses rough walls in greater detail.

Closing Comment

In our texts we attributed the friction factor defined by Eq. (17) to Darcy, as was common practice some years ago. In the late 1980's it became the practice to refer to the Darcy–Weisbach friction factor, because Weisbach had used Eq. (17) to define f in a paper published in 1845. However, the issue of an appropriate name for this factor is complicated: an excellent discussion of the pertinent history is given by Professor Glenn Brown of Oklahoma State University.

Briefly, Weisbach did introduce Eq. (17) to define f in 1845; however he did not provide adequate data for the evaluation of f and his crude prescription did not agree well with experiment. In fact, the earlier Prony equation was more accurate, and had the form

$$\Delta P = (L/D)(aV + bV^2) \tag{24}$$

where the constants a and b depend on the type of pipe. Subsequently in 1857, Darcy published an improved Prony equation based on a large experimental data base,

$$\Delta P = (L/D)\left[\left(c + \frac{d}{D^2}\right)V + \left(d + \frac{e}{D}V^2\right)\right] \tag{25}$$

where now c, d and e were for a given type of pipe. Notice that the Darcy e/D corresponds to ε/D the relative roughness parameter, which multiplies V^2 to correctly recognize that pressure drop in the fully rough regime is due to form drag on the roughness elements.

SUPPLEMENT

7

FLUX DEFINITIONS FOR MASS TRANSPORT

CONTENTS

1 Introduction 54
2 Mass and Molar Fluxes 54
3 Thermal Analogy to Mass Transport 56
4 Flaws in the Traditional Approach 56
5 Flow Model of Diffusion 57
6 Concluding Remarks 58
7 Acknowledgement 58

1 INTRODUCTION

It has been our experience that students have had considerable difficulty mastering fundamentals of chemical species transport in mixtures. One possible reason is that the traditional approach to the definitions of species fluxes in the United States is arguably flawed.

In the third editions of *Mass Transfer* and *Basic Heat and Mass Transfer* we have followed a different approach to defining species fluxes. At first sight our approach may not appear to be much different to past practice; but the subtle differences do have a profound impact on the understanding of the underlying physics. We present here the ideas that led to the changes in the third editions.

2 MASS AND MOLAR FLUXES

Many years ago, Maxwell explained that mass species transport was due to both motion caused by agitation and motion associated with translation. Expanding on this concept:

1. Diffusion is caused by random molecular motion that is a consequence of thermally induced agitation.
2. Convection is a macroscopic process in which portions of the medium are moved over much larger distances than those characterizing the diffusion process.
3. Diffusion and convection are distinct and independent physical transport mechanisms that sum to give a total mass transport flux.

On a mass basis we write the total mass transport flux $\mathbf{n}_i$ relative to laboratory coordinates as:

$$\mathbf{n}_i = m_i\mathbf{n} + \mathbf{j}_i = \rho_i\mathbf{v} + \mathbf{j}_i \qquad ; \qquad \sum \mathbf{j}_i = 0 \tag{1}$$

Since we are working on a mass basis, $\rho_i\mathbf{v}$ is the convective flux relative to laboratory coordinate system defining the vector $\mathbf{v}$. Likewise, $\mathbf{j}_i$ is the diffusion flux, also relative to laboratory coordinates; there are no other choices possible.

We can determine $\mathbf{j}_i$ from a physical transport model by setting $\mathbf{v} = 0$ to isolate diffusive transport. Using the kinetic theory of gases for a binary mixture, Fick's Law is obtained

$$\mathbf{j}_1 = -\rho\mathscr{D}_{12}\nabla m_1 \tag{2}$$

where the del operator is defined by the laboratory coordinate system. For a multicomponent mixture Eq. (2.214) and (2.215) of *Mass Transfer* in macroscopic form are:

$$\mathbf{j}_i = \frac{c^2}{\rho} \sum_{j=1}^{n} M_i M_j D_{ij} \mathbf{d}_j - D_i^T \nabla \ln T \tag{3a}$$

$$\mathbf{d}_j = \nabla x_j + (x_j - m_j) \nabla \ln P - \frac{m_j}{\mathscr{R} T} (\mathbf{f}_j - \sum_{k=1}^{n} m_k \mathbf{f}_k) \tag{3b}$$

Again note that $\mathbf{j}_i$, the diffusion flux, is relative to the coordinate system of the del operator and external force vectors: it is not relative to the mass average velocity.

Similarly, on a molar basis it is customary to write the total molar flux relative to laboratory coordinates as:

$$\mathbf{N}_i = x_i \mathbf{N} + \mathbf{J}_i^* = c_i \mathbf{v}^* + \mathbf{J}_i^* \quad ; \quad \sum \mathbf{J}_i^* = 0 \tag{4}$$

Since we are working on a molar basis, $c_i \mathbf{v}^*$ is the convective molar flow and $\mathbf{J}_i^*$ is the diffusive molar flux, both relative to laboratory coordinates.No other choices are possible. Note that $\mathbf{J}_i^*$ is not "relative" to the molar average velocity and thus the $*$ superscript is not necessary and is misleading. However, since use of the superscript is customary, it will be retained in this explanatory development.

$\mathbf{J}_i^*$ can also be obtained from the kinetic theory of gases. For a binary mixture we need only use the mass based result and algebra. Eq. (2) gives $\mathbf{j}_1$: then using $\mathbf{N}_i = \mathbf{n}_i / M_i$ and the definitions of $\mathbf{n}_i$ and $\mathbf{N}_i$ (Eqs. (1) and (5)) yields:

$$\mathbf{J}_1^* = -c \mathscr{D}_{12} \nabla x_1 \tag{5}$$

where the diffusion coefficient $\mathscr{D}_{12}$ is the one defined in the mass formulation, Eq. (2).

For a multicomponent system, algebra does not yield an explicit expression for $\mathbf{J}_i^*$: all we have are the Stefan-Maxwell (S-M) equations. These equations can be derived directly from the kinetic theory of gases [1, Section 7.4]. Since ordinary diffusion is the issue here, the S-M equations for an ideal gas mixture reduce to:

$$c \nabla x_i = \sum_j \frac{(x_i \mathbf{J}_j^*) - (x_j \mathbf{J}_i^*)}{\mathscr{D}_{ij}} \tag{6}$$

where the $\mathscr{D}_{ij}$ are the binary diffusion coefficients. For a binary mixture 1,2, Eq. **(6)** reduces to Fick's Law:

$$\mathbf{J}_1^* = -c \mathscr{D}_{12} \nabla x_1 \tag{7}$$

In practice we use the S-M equations to obtain the set of diffusion fluxes $\mathbf{J}_i^*$, and then use Eq. (5) to obtain the total fluxes. Once again we note that it is not necessary to use a * superscript on the $\mathbf{J}_i^*$ since they are independent of $\mathbf{v}_i^*$: they are the molar diffusion fluxes relative to laboratory coordinates.

3 THERMAL ANALOGY TO MASS TRANSPORT

The student of mass transfer has usually had prior exposure to convection heat transfer, and so the thermal analog to mass transport is instructive. We write:

$$\mathbf{q}(\text{or } \dot{\mathbf{e}}) = \rho \mathbf{v} h - k\nabla T \tag{8}$$

Both the convective flow and the conduction (diffusive) flux are relative to laboratory coordinates. If we wish to determine the thermal conductivity we can either:

1. Use a thermal conductivity cell where we ensure that $\mathbf{v} = 0$
2. Set $\mathbf{v} = 0$ in a physical model of energy transport. (In the kinetic theory of gases we determine k for a pure gas in this manner).

We have no need to say that the conduction flux is relative to the convective flow; both are relative to laboratory coordinates, and are independent. Of course, this concept is never questioned in heat transfer texts.

4 FLAWS IN THE TRADITIONAL APPROACH

The preceding development follows Maxwell by writing the total mass transport rate as the sum of a convective flow and a diffusive flux, surely a rather simple concept. The result is identical to that used in common practice. So why has there been confusion in the literature?

1. Much of the mass transport literature in the United States has origins in the writings of R.B Bird [2] where he presents an abstract mathematical framework of velocity and flux definitions. In particular he writes

$$\mathbf{v}_i = \mathbf{v} + \hat{\mathbf{v}}_i \tag{9a}$$

$$\mathbf{v}_i = \mathbf{v}^* + \hat{\mathbf{v}}_i^* \tag{9b}$$

where $\mathbf{v}_i$ is an absolute species velocity, $\hat{\mathbf{v}}_i$ is the diffusion velocity "relative" to the mass average velocity, $\mathbf{v}$, and $\hat{\mathbf{v}}_i^*$ is the diffusion velocity "relative" to the molar average velocity $\mathbf{v}^*$. Velocity vector diagrams are often drawn to reinforce the concept of a diffusion velocity being " relative" to a mixture average velocity. The problem with Eqs. (10a) and (10b) is that diffusion is a flux not a flow, and has no physically meaningful velocity associated with it [3]. To avoid this issue, Bird then uses corresponding flux definitions:

$$\mathbf{n}_i = \rho_i \mathbf{v} + \mathbf{j}_i \tag{10a}$$

$$\mathbf{N}_i = c_i \mathbf{v}^* + \mathbf{J}_i^* \tag{10b}$$

and states that $\mathbf{J}_i$ is relative to $\mathbf{v}$ and $\mathbf{J}_i^*$ is relative to $\mathbf{v}^*$. Since $\mathbf{J}_i^* = c_i \hat{\mathbf{v}}_i^*$, the use of the * superscript on $\mathbf{v}^*$ is introduced. But we have now seen that the diffusion

fluxes are relative to laboratory coordinates: the * superscript on $\mathbf{J}_i$ is unnecessary. The * superscript did allow Bird to distinguish between the following two mathematical expressions:

$$\mathbf{N}_i = c_i\mathbf{v} + \mathbf{J}_i \quad \textbf{(11a)}$$

$$\mathbf{N}_i = c_i\mathbf{v}^* + \mathbf{J}_i^* \quad \textbf{(11b)}$$

But Eq. **(11a)** makes no physical sense. Summing over all species, Eq. **(11b)** gives:

$$\sum \mathbf{N}_i = \mathbf{v}^* \sum c_i + \sum \mathbf{J}_i^* = c\mathbf{v}^* \quad \textbf{(12a)}$$

whereas, summing Eqs. **(11a)** gives

$$\sum \mathbf{N}_i = \mathbf{v} \sum c_i + \sum \mathbf{J}_i = c\mathbf{v} + \sum \mathbf{J}_i \quad \textbf{(12b)}$$

Since $\mathbf{v}^* \neq \mathbf{v}$, $\sum \mathbf{J}_i \neq 0$. Diffusion fluxes that do not sum to zero cannot represent a physical diffusion phenomenon: the $\mathbf{J}_i$ are mathematical abstractions of no value.

2. The work of Taylor and Krishna [4] is another quoted source for basic equations of mass transport. These authors have stated "The diffusive flux is defined as the difference between the total and convective fluxes. It is only defined once we have chosen a convective flux" . This statement is clearly influenced by the Bird formulation discussed above.Again the only valid mass diffusion flux is $\mathbf{j}_i$ given by Eqn. (2) and Eqn. (3); the only valid molar diffusion flux is $\mathbf{J}_i^*$ given by Eqn. (6) and (7). The flux $\mathbf{J}_i$ defined by (12a) is not a diffusion flux since $\sum \mathbf{J}_i \neq 0$
3. In most textbooks the student is introduced to simultaneous diffusion and convection in the analysis of the Stefan tube, which involves diffusion and induced convection. The diffusion of the carrier gas down the the tube is balanced by a convective flux driven by an induced pressure gradient. From the equations used in the analysis it is surely obvious to the student that the diffusion is relative to a coordinate system attached to the tube. How then can the concept of diffusion relative to the mass or molar average velocity makes any sense in this context? The student should be puzzled indeed.
4. Whereas the mass average velocity is a measurable physical quantity, the molar average velocity is not. It is simply a convenient mathematical concept that facilitates analysis of a limited subset of problems involving simultaneous diffusion and convection in isothermal system.

5 FLOW MODEL OF DIFFUSION

The kinetic theory of gases show very clearly that diffusion is not a flow and rather it is a *flux*. In a flow *model* of diffusion, species and diffusion velocities are defined as mathematical concepts, but have no physical meaning. Flow models of diffusion have been used for convenience: indeed there are three examples in *"Mass Transfer"*.

1. Equation (2.238) for muticomponent diffusion in liquids involves species velocities $\mathbf{v}_i$ following standard practices in physical chemistry and chemical engineering. Equation (2.238) must be used with care since $\mathbf{v}_i$ becomes singular where the concentration of species i goes to zero.
2. Equation (2.248) for the diffusion creep velocity was derived using a flow model of diffusion. However a similar equation can be derived from the kinetic theory of gases in a manner similar to that used by Maxwell to derive the thermal creep velocity.
3. In Section 2.7.2, diffusion and energy flux vectors are taken, directly from the standard reference Hirschfelder, Curtiss and Bird [2] and are written in terms of the species diffusion velocity $\mathbf{v}_i$. In particular, the Stefan-Maxwell equations, Eq (2.218) are also written in terms of diffusion velocities, and are also often seen written in terms of species absolute velocities. Since:

$$(\hat{\mathbf{v}}_j - \hat{\mathbf{v}}_i) = (\mathbf{v}_j - \bar{\mathbf{v}}) - (\mathbf{v}_i - \bar{\mathbf{v}}) = (\mathbf{v}_j - \mathbf{v}_i)$$

the result is similar to the equations used for multicomponent diffusion in liquids (Eqn. 2.238), obtained from a flow model of diffusion . However, the kinetic theory does not invoke a flow model: Eqn. (2.218) is obtained from Eqn. (2.214) by algebra alone. The use of the diffusion velocity does give more compact equations, but as mentioned before, it must be used carefully since it has no physical reality.

6 CONCLUDING REMARKS

In summary we are making two recommendations:

1. The essentially abstract formulation of Bird should be abandoned and replaced by Maxwell's concept to yield a physics based formulation of mass transport in mixtures.
2. The basic flux relations remain unchanged; however we should cease use of the * superscript on $\mathbf{J}_i^*$ since it is misleading and unnecessary.

7 ACKNOWLEDGEMENT

The authors thank Professors J.H. Lienhard V and R. Greif for helpful discussions.

REFERENCES

1. R Byron Bird. Theory of diffusion. *Advances in chemical engineering*, 1:156–239, 1956.

2. Joseph O Hirschfelder, Charles F Curtiss, Robert Byron Bird, and Maria Goeppert Mayer. *Molecular theory of gases and liquids*, volume 26. Wiley New York, 1954.

3. AF Mills. The use of the diffusion velocity in conservation equations for multicomponent gas mixtures. *International journal of heat and mass transfer*, 41(13):1955–1968, 1998.

4. Ross Taylor and Rajamani Krishna. *Multicomponent mass transfer*, volume 2. John Wiley and Sons, 1993.

SUPPLEMENT

8

THE OCEAN SURFACE ENERGY BALANCE

CONTENTS

1 Introduction 62
2 Temperature profiles in the tropical ocean 62
3 The energy balance at night 63
4 The energy balance in daytime 65
5 The transient problem 65
6 Solution of the balance equation 65
7 Effect of ocean temperature on heat loss 67
8 Effect of sky radiation on "heating" the ocean 69
9 Specification of the ocean surface temperature 72
10 The approximation $T_s = T_b$ 73

1 INTRODUCTION

More than 70% of the earth's surface is water, primarily in the oceans. Current concern about global warming and climate change has led the science community to have considerable interest in the thermal behavior of the oceans, and in the measurement of the ocean surface temperature. To obtain an understanding of the phenomena involved, we need to characterize the temperature profiles adjacent to the ocean-air interface and the associated heat transfer processes. The interface energy balance should be then quantified and the interface temperature behavior investigated. Subsequently we can examine the consequences for ocean warming, and for the measurement of the ocean surface temperature.

Surface energy balances for an evaporating water surface were dealt with in Chapter 9 of BHMT and Chapter 1 of MT. Students found it to be a complicated subject that took considerable effort to master. The ocean surface energy balance is no exception! There are many complicating factors that will not be discussed in this supplement. Our goal here is to use the fundamental heat and mass transfer methodology used in our textbooks to draw a sketch of the interface processes that are most relevant. The highly transient shape and properties of the turbulent air-sea interface and the presence of foam, bubbles, salt aerosols, and other relevant processes will not be considered in detail. The following analysis is based on time-averaged processes over diurnal or even decadal length scales.

Our starting point is Eq. (9.55) of BHMT (or Eq. (1.55) of MT), which gives the surface energy balance for water evaporating into air as

$$-k\frac{\partial T}{\partial y}\bigg|_u = h_c(T_s - T_e) + g_{m1}(m_{1,s} - m_{1,e})h_{\text{fg}} + q_{\text{rad}} \qquad \textbf{(1)}$$

where h_c and g_{ml} are convective transfer coefficients on the air side of the interface.

2 TEMPERATURE PROFILES IN THE TROPICAL OCEAN

The first step is to sketch expected temperature profiles on each side of the interface, as shown in Fig. 1. Two cases have to be considered, (a) nighttime, and (b) daytime. The night profile is simpler: the water temperature is relatively constant with depth down to 50-200 m (depending on water conditions), except for a very thin (1–5 mm) thermal boundary layer adjacent to the interface where it decreases to the interface temperature T_s. This decrease is required to transport enthalpy of vaporization to the water evaporating at the interface.

The day profile is not monotonic. Short wavelength solar radiation penetrates the water, but attenuates over a depth of about 10 m. The absorption of this radiation decreases exponentially below the interface leading to a temperature that decreases with increasing depth. However, as for the nighttime, enthalpy of vaporization must be transported to the evaporating surface, also requiring a temperature gradient. A temperature maximum results about 5 mm below the interface (see [1] for more details). With strong winds the day profile approaches the night profile due to more intensive convective mixing. The air temperature T_e is usually lower than T_s over the open ocean, but the difference depends on weather and wind conditions.

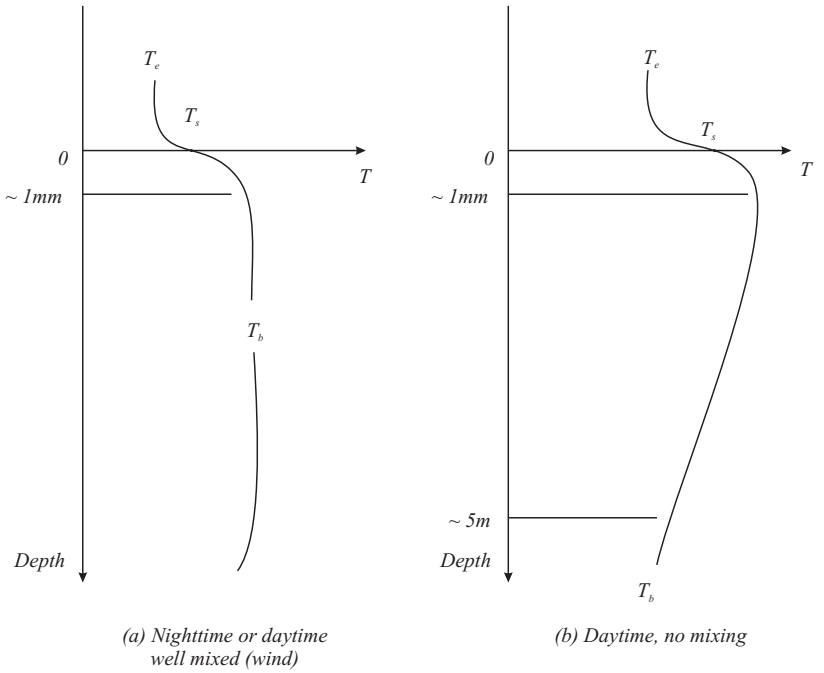

Figure 8.1: Expected temperature profiles on each side of the ocean-air interface, (a) nighttime, (b) daytime.

3 THE ENERGY BALANCE AT NIGHT

To proceed, we examine each term in the equation. Heat transfer from the bulk water to the interface can be characterized by a convective heat transfer coefficient,

$$-k\frac{\partial T}{\partial y}\bigg|_u = h_{cL}(T_b - T_s) \tag{2}$$

where h_{cL} is the convective heat transfer coefficient on the water side of the interface, and T_b is the bulk temperature of the ocean at an appropriate depth. When there is little wind, there is a natural convection flow below the interface driven primarily by the temperature variation. But the effect of wind is to agitate the interface to form waves and associated complex secondary motions. At present we need to rely on experimental data for h_{cL} and fortunately some such data are available for a range of wind speeds.

Convective heat transfer from the interface to the air can be characterized by a heat transfer coefficient h_c, which is also very dependent on wind speed. Similarly the mass transfer conductance g_{m1} depends on wind speed, and is related to h_c by the heat and mass transfer analogy. As for h_{cL}, we must rely on experimental data for h_c, and data available is adequate for our purposes. Table 1 presents representative values for the three transfer coefficients.

	h_{cL} (W/m^2 K)	h_c (W/m^2 K)	$g_{\rm ml}$ (kg/m^2 s)
1. Still-natural convection	216	3.2	0.00034
2. Wind speed 3 m/s	420	4.0	0.0036
3. Wind speed 5 m/s	1050	10	0.011
4. Wind speed 10 m/s	3600	18	0.024

Table 1: Transfer coefficients at the ocean surface. Various sources, in particular [7].

The radiation heat flux $q_{\rm rad}$ can be obtained from Eq. (6.54) of BHMT, BHT, or HT,

$$q_{\rm rad} = \varepsilon E_b - \alpha_s G_s - \alpha G \tag{3}$$

The control volume surrounding the interface used to derive Eq. (1) is vanishingly thin, so it can be assumed to be transparent to shortwave solar radiation: thus in general we can put $\alpha_s = 0$ in Eq. (3). Alternatively, we can simply take $G_s = 0$ at night. Modeling the effect of long wavelength radiation G in Eq. (3) is more subtle. The extinction depth of long wavelength thermal radiation in water is of the order of 0.1 mm, which we can assume small compared to the thickness of the thermal boundary layer associated with h_{cL}. Thus we *model* the absorption of thermal radiation as a surface phenomenon with absorptivity α taken equal to ε for a gray surface. Equation (3) with $G = J_{\rm sky}$ for a shape factor of unity, becomes

$$q_{\rm rad} = \varepsilon\sigma T_s^4 - \alpha J_{\rm sky} \tag{4}$$

The sky radiation $J_{\rm sky}$ is often called the *back radiation* in climate science. It is the downwelling longwave radiation from the atmosphere, primarily from *greenhouse gases*, including water vapor, carbon dioxide, ozone, methane, etc., and from low level clouds if the sky is not clear. Referring to Eq. (6.51) of BHMT, we can introduce a *sky emittance* and write

$$J_{\rm sky} = \varepsilon_{\rm sky}\sigma T_e^4 \tag{5}$$

where T_e is approximated as the ocean level air temperature. In practice, we use experimental data for the back radiation to develop correlations for $\varepsilon_{\rm sky}$, for example the Brunt correlation Eq. (6.52) in BHMT. Improved forms of the Brunt correlation have recently been proposed by Li, Jiang and Coimbra [2]. For the clear nighttime sky they propose

$$\varepsilon_{\rm sky} = 0.633 + 0.0057(P_{1,e})^{1/2}; \quad P_{1,e} \text{ in pascals.} \tag{6}$$

Substituting the Eq. (1) then gives the surface energy balance at night as

$$h_{cL}(T_b - T_s) = h_c(T_s - T_e) + g_{m1}(m_{1,s} - m_{1,e})h_{\rm fg} + \varepsilon\sigma T_s^4 - \alpha\varepsilon_{\rm sky}\sigma T_e^4 \tag{7}$$

An examination of the right side of Eq. (7) shows that it is always positive – as follows. Looking at the dominant terms first, the evaporation heat loss is always positive since $m_{1,s}$ is always greater than $m_{1,e}$. The net radiation contribution is always positive since $\varepsilon_{\rm sky} \sim 0.8{-}0.9$: for it to be negative T_e should exceed T_s by more

than about 8 K, which never happens over the open ocean. The heat convection term is positive for $T_s > T_e$, but even if $T_s < T_e$, the value of the term proves to be small compared to the positive terms on the right side of Eq. (7). Thus we can state that the ocean always loses heat to the atmosphere at night. Indeed, the ocean always loses heat to the atmosphere during the daytime as well.

4 THE ENERGY BALANCE IN DAYTIME

Figure 1.b shows the daytime temperature profile which results from solar radiation being absorbed over a penetration depth of about 10 m. We can no longer characterize the convective heat transfer to the interface by a simple convective heat transfer coefficient. The heat transfer problem involves simultaneous convective and radiative transfer, a topic not covered in elementary heat transfer texts. However, a simple qualitative discussion will suffice.

As for the nighttime case, we can again note that the right side of Eq. (7) is always positive, indicating a heat loss from the ocean to the atmosphere, with the associated temperature profile in the ocean adjacent to the interface shown in Fig. 1.b. The absorption of solar radiation leads to the maximum temperature shown, and heat is transported both upwards to the ocean surface and downwards to a well-mixed lower layer.

5 THE TRANSIENT PROBLEM

Figure 1 showed instantaneous temperature profiles near the interface. Figure 2 shows an in-depth temperature profile with a surface layer and the *thermocline* where the temperature decreases to values found in the deep ocean. Heating and cooling of the surface layer is a periodic heat transfer problem: this layer warms during the day and cools during the night. Over this cycle the layer continuously loses heat to the deep ocean and the ocean surface.

There are also variations with latitude, the seasons, and due to ocean currents. Warmer surface water tends to flow from the tropics to the poles, for example, the North Atlantic Drift current. The El Nino phenomenon induced by strong trade winds causes cold water to upwell in the eastern Pacific Ocean and warm water to accumulate in the western Pacific. The deep ocean is in a quasi-steady state, and not much is known about the details of deep ocean currents and their long time scales. There is net heat intake in the tropics and net heat rejection at high latitudes. Notwithstanding these complications, the surface interface balance operates in much the same way everywhere.

6 SOLUTION OF THE BALANCE EQUATION

We will first consider nighttime conditions for which Eq. (7) can be rearranged as

$$a\varepsilon_{\text{sky}}\sigma T_e^4 + h_{cL}(T_b - T_s) = \varepsilon\sigma T_s^4 + h_c(T_s - T_e) + g_{m1}(m_{1,s} - m_{1,e})h_{\text{fg}} \qquad \textbf{(8)}$$

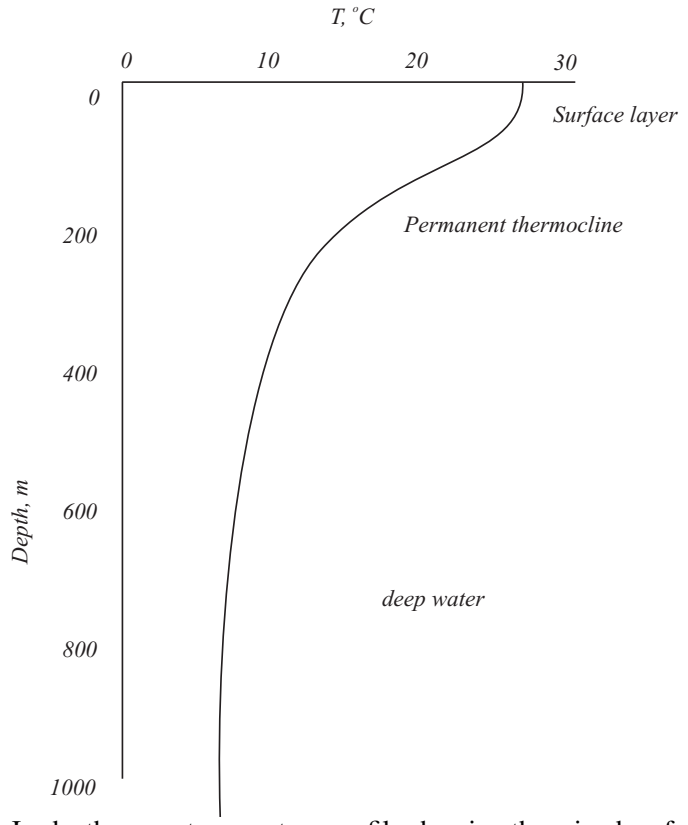

Figure 8.2: In-depth ocean temperature profile showing the mixed surface layer and the thermocline.

The left side contains heat fluxes into the interface control volume, while the right side contains heat fluxes out the control volume. We also have vapor pressure data that can be represented by a second equation,

$$m_{1,s} = m_{1,s}(P, T_s) \quad h_{\text{fg}} = h_{\text{fg}}(T_s) \qquad \textbf{(9 a,b)}$$

Given values of T_e, $m_{1,e}$ and T_b, together with data (formulas) for the transfer coefficients, Eqs. (8) and (9) can be solved. Many exercises and examples in BHMT and MT involved similar situtations. An iterative solution procedure was used to determine the unknown interface temperature T_s (and $m_{1,s}$). Then the various heat fluxes could be calculated and compared.

However the parameters T_e, $m_{1,e}$ and T_b are time dependent (diurnal, seasonal) and location dependent. To explore the behavior of the surface fluxes, we could perform parametric calculations: because iteration is required, a computer program is indicated for such a task.

We will first obtain the energy balance for a base case typical of the tropics. We specify:

$P = 1$ atm, $T_e = 296$ K, R.H. = 75%, $T_b = 300.5$ K, and a wind speed of 3 m/s. Using Tables A.12a of the texts, and Table 1 of this supplement,

$P_{1,\text{sat}}(296\,\text{K}) = 2783\,\text{Pa}$; $P_{1,e} = (0.75)(2783) = 2087\,\text{Pa}$
$m_{1,e} = 0.01306$; $h_{\text{fg}}(300\,\text{K}) = 2.44 \times 10^6\,\text{J/kg}$
Using the modified Brunt equation Eq. (6) gives

$$\varepsilon_{\text{sky}} = 0.893; \text{ also } a = 0.9 = \varepsilon$$

$$h_{cL} = 420\,\text{W/m}^2\text{K}; \quad h_c = 4.0\,\text{W/m}^2\text{K}; \quad g_{m1} = 3.6 \times 10^{-3}\,\text{kg/m}^2\text{s}$$

$$a\varepsilon_{\text{sky}}\sigma T_e^4 = (0.9)(0.893)(5.67 \times 10^{-8})(296^4) = 349.8\,\text{W/m}^2$$

$$\varepsilon\sigma T_s^4 = (0.9)(5.67 \times 10^{-8})T_s^4 = 5.103(T_s \times 10^{-2})^4\,\text{W/m}^2$$

$$g_{m1}h_{\text{fg}} = (3.6 \times 10^{-3})(2.44 \times 10^6) = 8784\,\text{W/m}^2$$

Choosing $T_s = 300.0$ K as a first guess,

$$349.8 + 210 = 413.3 + 16 + 80.2$$

$$559.8 \neq 509.5$$

After a few trials, choose $T_s = 300.11$ K

$$349.8 + 163.8 = 413.94 + 16.44 + 80.65$$

$$513.6 = 511.0$$

Which is as close as one can obtain without going to the next significant figure for T_s. So what does this balance tell us?

1. The relative magnitudes of the terms on the right side of the equation allow us to compare the three heat losses from the surface.

   $$\text{emission/convection/evaporation} = 81.0/3.22/15.8\,\%$$

   that is, the heat loss is dominated by radiation emission, with evaporation a factor of 5 less.
2. The three losses from the interface balance the sky radiation absorbed at (close to) the interface, plus the heat loss from the bulk ocean.
3. The energy balance controls the interface temperature, which then sets the magnitudes of the ocean heat loss and the three losses to the atmosphere: The sky radiation $\varepsilon_{\text{sky}}J_{\text{sky}}$ is, of course, independent of T_s.
4. The value of $(T_b - T_s) = 0.39$ K is in good agreement with the data of Robertson and Watson [1].

7 EFFECT OF OCEAN TEMPERATURE ON HEAT LOSS

The "bulk" ocean temperature, T_b in Eq. 8, is not constant: in particular there is a diurnal variation with T_b increasing during the day due to absorption of solar radiation, and decreasing at night. Let us redo the surface energy surface balance for $T_b = 301.0$ K, an increase of 0.5 K over the value used in the base case solution already obtained. We could redo the balance for the new value of T_b, but it is simpler

and instructive to obtain the solution by perturbation. The energy balance used in the base case was

$$349.8 + 420(T_b - T_s) = 5.103(T_s \times 10^{-2})^4 + 4(T_s - 296) + 8784(m_{1,s} - 0.01292) \quad \textbf{(10)}$$

Now perturb T_b to T_b' and subtract Eq. (10)

$$420(T_b' - T_b) = 5.103 \times 10^{-8}(T'^4_s - T_s^4) + 4(T_s' - T_s) + 8784(m_{1,s}' - m_{1,s}) + 420(T_s' - T_s) \quad \textbf{(11)}$$

Since $\Delta T_s = T_s' - T_s$ will be small, we can linearize the emission and evaporation terms,

$$5.103 \times 10^{-8}(T'^4_s - T_s^4) = (5.103 \times 10^{-8})(4)(T_s^3)(T_s' - T_s) = 5.515\,\Delta T_s$$

$$8784(m'_{1,s} - m_{1,s}) = 8784(dm_1/dT_s)_{300\,\mathrm{K}}\,\Delta T_s = 11.33\,\Delta T_s$$

Substituting in Eq. (11)

$$(420)(0.5) = 5.515\Delta T_s + 4\Delta T_s + 11.33\Delta T_s + 420\Delta T_s$$

$$210 = 440.8\Delta T_s$$

$$\Delta T_s = 0.476\,\mathrm{K}$$

Thus $T_s = 300.11 + 0.476 = 300.59$ K, and computing the fluxes gives

	Base case	Perturbed	Δ
T_b (K)	300.5	301.0	0.5
T_s (K)	300.11	300.59	0.48
q_L (W/m^2)	163.8	172.2	8.4
q_{emm} (W/m^2)	413.94	416.6	2.66
q_{sens} (W/m^2)	16.44	18.36	1.92
q_{evap} (W/m^2)	80.65	86.62	5.97

When T_b is increased an increase in T_s follows to allow the change in heat loss from the ocean to balance the change in heat loss into the atmosphere. The changes are nearly linear and easily understood. That is, the interface temperature essentially "tracks" the bulk temperature.

The previous analysis considers a step change in T_b, with T_e and $m_{1,e}$ held constant. But as T_b and T_s change in a diurnal cycle, so will T_e and $m_{1,e}$ due to heat and mass transfer from the interface and heating/cooling of the air boundary layer. This is a more complex problem but is not really relevant to our observation that the interface temperature tracks the bulk ocean temperature.

8 EFFECT OF SKY RADIATION ON "HEATING" THE OCEAN

An issue that has been troublesome on climate blogs is the effect of sky radiation "heating" the ocean. The word heating is in quotes here because we will see that it may be a misleading concept. Of concern has been the effect of increasing *greenhouse* gases, in particular, CO_2. A first order effect of increasing CO_2 in the atmosphere is via an increase in the sky radiosity $J_{\text{sky}}(=\varepsilon_{\text{sky}}\sigma T_e^4)$, which in our model requires increasing ε_{sky}. However, the pertinent literature on the heating effect of CO_2 usually does not involve ε_{sky}: rather it simply uses values of J_{sky}. We will do a perturbation analysis with a nominal 1 W/m^2 change in $q_{\text{sky}} = \varepsilon J_{\text{sky}}(\alpha = \varepsilon)$; we will see later that, by chance, this change corresponds to the actual change of about 100 ppm CO_2 over 100 years. Note that this apparently small change is cumulative over time, so that an average forcing of 1 W/m^2 does add up to a measurable contribution.

We used the energy balance in the following form to obtain $T_s = 300.06$ K:

$$q_{\text{sky}} + 420(300.5 - T_s) = 5.103(T_s \times 10^{-2})^4 + 4(T_s - 296) + 8784(m_{1,s} - 0.01292) \quad \textbf{(12)}$$

Now perturb q_{sky} to q'_{sky}, for which T_s will change to T'_s, and subtract Eq. (12)

$$q'_{\text{sky}} - q_{\text{sky}} + 420(T_s - T'_s) = 5.103 \times 10^{-8}({T'}_s^4 - T_s^4) + 4(T'_s - T_s) + 8784(m'_{1,s} - m_{1,s}) \quad \textbf{(13)}$$

Again we will linearize the emission and evaporation terms, and take $(q'_{\text{sky}} - q_{\text{sky}}) =$ 1 W/m^2 to obtain

$$1 - 420\Delta T_s = 5.515\Delta T_s + 4\Delta T_s + 11.33\Delta T_s; \quad \Delta T_s = T'_s - T_s \quad \textbf{(14)}$$

Solving, $\Delta T_s = 2.268 \times 10^{-3}$ K ($\sim$0.00227 K). The corresponding changes in the fluxes and the new values are

$$\Delta q_L = 0.953\,\text{W/m}^2; \qquad q'_L = 164.8\,\text{W/m}^2,$$

$$\Delta q_{\text{evap}} = 0.0257\,\text{W/m}^2; \qquad q'_{\text{evap}} = 80.68\,\text{W/m}^2,$$

$$\Delta q_{\text{emm}} = 0.0125\,\text{W/m}^2; \qquad q'_{\text{emm}} : \text{no significant change},$$

$$\Delta q_{\text{sens}} = 0.00905\,\text{W/m}^2; \qquad q'_{\text{sens}} : \text{no significant change}.$$

Of the increase in q_{sky} of 1 W/m^2, 95.3% goes to reduce the heat loss from the ocean, 2.57% goes to increased evaporation, 1.25% goes to increased emission, and 0.94% goes to increased sensible heat loss.

To call the reduction in heat loss from the ocean a "heating" of the ocean is perhaps simply an issue of semantics, but this terminology has caused confusion in the literature. Of greater concern is the misconception that, because the long wavelength sky radiation is absorbed in a few microns below the interface, this radiation cannot "heat" the deeper ocean: if is often claimed that it goes mainly to evaporation. Our balance shows that only 2.57% of a change in sky radiation goes to increased evaporation: 95.3% goes to reduce the heat loss from the ocean ("heat" the ocean). The important lesson to be learned from these calculations is that an understanding

of heat fluxes at the ocean surface requires that quantitative interface balances be performed. Too often in the literature statements are made that seriously violate the basic thermodynamics and heat transfer involved in the energy balance.

Of interest is how ε_{sky} must change to cause a 1 W/m^2 change in sky radiosity.

$$q_{\text{sky}} = a\varepsilon_{\text{sky}}\sigma T_e^4, \quad \text{thus } q'_{\text{sky}}/q_{\text{sky}} = \varepsilon'_{\text{sky}}/\varepsilon_{\text{sky}}$$

For $q_{\text{sky}} = 349.8$ W/m^2, $q'_{\text{sky}} = 350.8$ W/m^2, $\varepsilon_{\text{sky}} = 0.893$

$$\varepsilon'_{\text{sky}} = (350.8/349.8)(0.893) = 0.8956$$

The increase is 0.0026, or 0.29%

Values for ε_{sky} may be obtained from correlations of q_{sky} (e.g. the Brunt equation). Examination of the data used to produce such correlations shows scatter of the order of 0.02. To discern a trend of 0.0026 due to change in greenhouse gas concentrations would be very challenging.

The effect of CO_2 on ε_{sky} (or q_{sky}) depends strongly on the concentration of H_2O in the atmosphere, which varies greatly. A thorough discussion of this topic is beyond the scope of this supplement, and brief comments must suffice. A early relevant paper was that of Staley and Jurica [3], which used a theoretical model of radiation transport in the atmosphere to give data for ε_{sky} as a function of H_2O, O_3 and CO_2 concentrations. Recently, Coimbra and coworkers have obtained extensive results using spectrally resolved data for all major constituents of the atmosphere [2,4,5]. Figure (8.3) clearly shows the effect of water vapor content on the role played by CO_2. In order to carefully analyze the spectral contribution of each atmospheric constituent, the longwave spectrum is divided into seven bands: four absorbing bands and three window (non-absorbing) bands. The window bands allow longwave radiation from the ground and from the atmosphere to escape to outer space. The contributions to band j coming from atmospheric constituent i is defined as

$$\varepsilon_{\text{sky},ij} = \varepsilon_{\text{sky},i}(\Delta\nu_j) \tag{15}$$

where $\Delta\nu_j$ represents the range of wavenumbers within the band j.

The two absorbing bands of water vapor are (b1) 0–400 cm^{-1} and (b5) 1400–2250 cm^{-1}. The two absorbing bands of CO_2 are (b3) 580–750 cm^{-1} and (b6) 2250–2400 cm^{-1}. The three window bands (b2), (b4) and (b7) appear in between the absorbing bands. The band boundaries were carefully selected so that only the contribution of water vapor is shown in (b1), (b2), (b5) and (b7), and the contribution of CO_2 is only evident in bands (b3), (b4) and (b6). Figure (8.3) shows the contributions in each band from each atmospheric constituent with respect to the normalized partial pressure of water vapor p_w at the screening level above the surface ($p_w = P_w/P_0$ where $P_0 = 1.013 \times 10^5$ Pa). The contributions from bands (b6) and (b7) are small because little longwave is emitted in those wavenumber ranges according to Planck's law. A small amount of water vapor saturates bands (b1) and (b5) so that the contribution of water vapor does not increase with p_w and the contributions from other constituents are nearly zero in these two bands. For band (b2), the contribution of water vapor increases with increased p_w then becomes saturated when $p_w > 0.01$. The contributions from other constituents are negligible in (b2). Water vapor and CO_2 saturate band (b3), so the total contribution of H_2O and CO_2 plus the overlaps

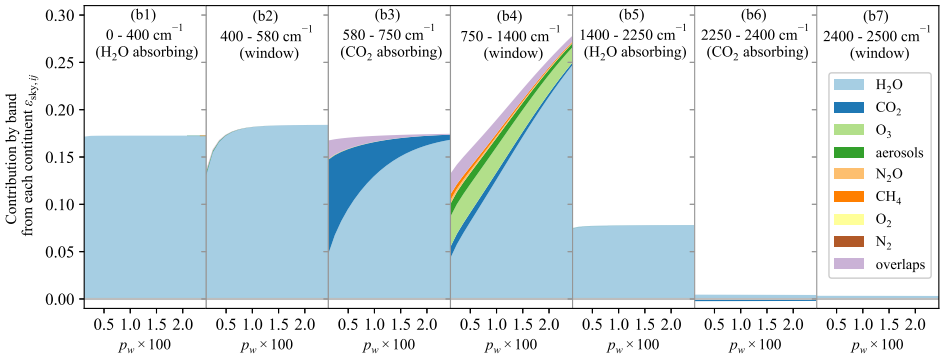

Figure 8.3: Contributions to the effective sky emissivity by atmospheric wavenumber band for each of the main atmospheric constituents. Note that band (b3) saturates rather easily with the current concentrations of CO_2 even at relatively low water vapor concentrations. Band (b4) is the main window for longwave radiation, and remains unsaturated even for very high concentrations of water vapor).

between the two absorbing spectra is nearly invariant with p_w. The contributions of O_3, N_2O, CH_4 and aerosols are only relevant in band (b4), the so-called *atmospheric window*. As expected, the contribution of water vapor increases with increased values of p_w while the relative contributions from other constituents decrease. Note that band (b4) is not saturated even when very high water vapor content is present in the atmospheric column. The spectral extinction coefficients for each main constituent of the clear atmosphere are plotted in Fig. 8.4, where the absorbing bands of water vapor (light blue) and CO_2 (dark blue) are readily identifiable. These results for clear skies (not including clouds) indicate that the effects of increasing CO_2 concentrations are more strongly felt over drier areas, which include high latitude land and ocean covered with ice, and also high altitude land with snow cover. These results also show the potential for strong feedback processes if the values of J_{sky} in those areas are high enough to melt the high albedo snow or ice cover, thus exposing low albedo land (rock and soil) or water. To further complicate things, the processes of cloud formation and transport are also strongly dependent on water concentrations at the lower layers of the atmosphere, including the humidity levels of the soil.[1]

For example, a sample calculation gave an increase in q_{sky} due to a 100 ppm increment of CO_2 of 1.2 W/m^2 for drier conditions (say over dry land), but only 0.3 W/m^2 for wetter conditions (say over the tropical ocean). Direct measurement of the contribution of CO_2 to q_{sky} is difficult and there are few data sets available. However Feldman et al. [6] measured q_{sky} at two continental U.S. locations from 2000 to 2010 to obtain an increase of 0.2 ± 0.07 W/m^2 for a 22 ppm increase in atmospheric CO_2, i.e., about 1 W/m^2 per 100 ppm CO_2.

[1] A particularly strong factor in low cloud formation over land is the Bowen ratio, which is a dimensionless number commonly used in meteorology and hydrology that is closely related to the Jakob number defined in Eq. (3.90) of HT.

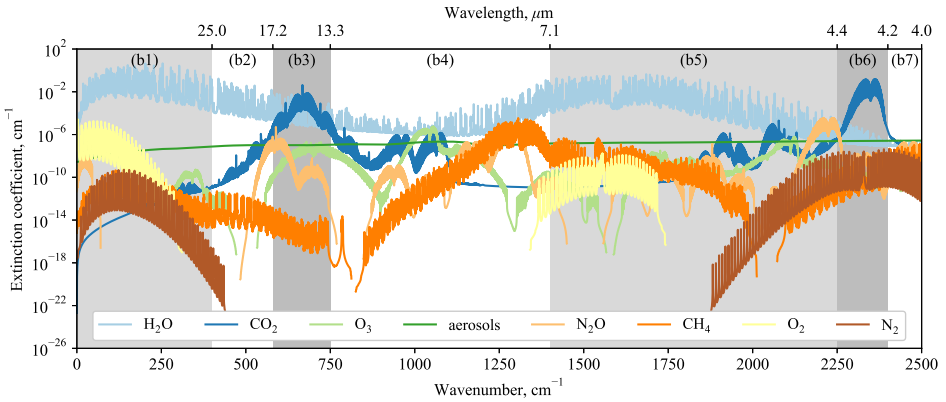

Figure 8.4: Spectral extinction coefficients for main atmospheric constituents at the lowest layer of the troposphere. The absorption coefficients (κ_λ) (see Section 6.7 of HT) are obtained from the HITRAN database and from the MT_CKD continuum model. The extinction coefficients of aerosols are calculated using Mie theory [5].

9 SPECIFICATION OF THE OCEAN SURFACE TEMPERATURE

With our understanding of the ocean surface energy balance and the role it plays in controlling the ocean-air interface temperature, we can now examine issues related to measurement of ocean surface temperature. The specification of a "global average surface temperature" (GAST) has been central to discussions of global warming and its possible mitigation. The focus is usually on the "GAST anomaly", that is the average departure of surface temperatures from reference values for a chosen base period, often 1981–2010. Since oceans cover more than 70% of the earth's surface, it is necessary to properly characterize and measure the ocean surface temperature to calculate the GAST anomaly.

To conform with practice for land surface temperature measurement, we might suggest that the air temperature 1.25–2.0 m about the ocean surface should be measured: but that is clearly impractical. So what has been measured? Common practice has been to use a "sea surface temperature" or SST that has been measured in various ways. Early measurements were made with bucket samples taken over the side of ships: a mercury thermometer was placed in the retrieved bucket to obtain a water temperature. (An error analysis of this procedure is an interesting exercise for the student!) Starting around World War II, temperatures were measured in cooling water intakes of ships engines, but for purposes of engine management rather than for meaningful and accurate surface temperature measurement. Also, these measurements were restricted to the main shipping lanes, a very small fraction of the ocean surface. More recently we rely on "drifting buoys" which measure the water temperature about 10 cm below the water-air interface. The Argo floats are also used, but the main purpose of this very sophisticated buoy array is to obtain temperature profiles down to 2000 m below the ocean surface.

Clearly, the so called surface water temperature measured by these techniques is poorly defined. Yet it is claimed that it is an appropriate proxy for the air temperature above the surface of the ocean, and can be combined with air temperatures measured

over land to obtain data for the GAST anomaly. From our examination of ocean temperature profiles we know that these measurements are of temperatures in the bulk surface layer outside the thermal boundary layer below the ocean interface. Yet it is claimed that it is a good approximation to the air temperature above the ocean even though the air can only respond to the interface temperature and conditions above the ocean. The measured temperatures are higher than the interface temperature so this claim must be rationalized in one of two ways:

1. The difference between T_s and the bulk temperature measured by the buoys can be neglected.
2. By chance, the air temperature above the ocean is higher than the interface temperature by the same amount as the bulk water temperature below the interface.

These combined sea-land temperature anomalies are call "blended" data sets.

Less widely used are actual measurements of the air temperature, made usually on the bridge of ocean-going ships (with appropriate correction for height above the interface). Nighttime values are used to avoid solar effects on the measurements. These "NMAT" data sets are used in some estimates of the GAST anomaly. It is of interest to note that although NMAT data have received attention, data for the marine air humidity is almost non existent. Our examination of the ocean surface energy balance shows that the humidity plays a much more significant role than temperature due to its effect on evaporation rates.

Section 10 of this supplement explores the consequence of assuming that the interface temperature equals the bulk water temperature.

10 THE APPROXIMATION $T_s = T_b$

As we have noted already, common practice has been to ignore the thermal boundary layer in the ocean and approximate the interface temperature T_s by a bulk temperature T_b. We can use the results of ocean surface energy balance to assess the consequences of this approximation. Referring to the base case of the nighttime energy balance, we can recalculate the surface fluxes for $T_s = T_b = 300.5$ K to obtain the following values:

	$T_s = 300.11$ K	$T_s = 300.5$ K	Δq
q_{emm} (W/m^2)	413.9	416.1	2.2
q_{sens} (W/m^2)	16.1	18.0	1.9
q_{evap} (W/m^2)	80.9	83.8	3.1
			$\sum$7.2

Perhaps we should also recalculate q_{sky} for an increase in T_e of 0.39 K; then $\Delta q_{\text{sky}} = 1.8$ W/m ^{2}, and we could say that the error caused by using T_b is $(7.2 - 1.8) = 5.4$ W/m^2. So we conclude that there are bias errors of $5.4 - 7.2$ W/m^2 introduced into the surface energy balance by approximating T_s by T_b.

REFERENCES

1. Roberston, J.E., and Watson, A.J., "Thermal skin effect of the surface ocean and its implications for CO_2 uptake." Nature, 358, 738–740 (1992).

2. Li, M., Jiang, X., and Coimbra, C.F.M., "On the determination of atmospheric longwave length irradiance under all sky conditions" *Solar Energy*, 144, 40–48 (2017).

3. Staley, D.O., and Jurica, G.M., "Effective atmospheric emissivity under clear skies" *J. Applied Meterology*, 11, 349–356 (1972).

4. Coimbra, C.F.M., Li, M., and Zhouyi, L. "Efficient model for evaluation of spectral and vertical distributions of atmospheric longwave radiation". Proc. 16th International Heat Transfer Conference, IHTC-16. August 10–15, Beijing (2018).

5. Li, M., and Coimbra, C.F.M., "On the effective spectral emissivity of the sky" *Private Communication* (2018).

6. Feldman, D.R., Collins, W.D., Gero, P.J. Torn, M.S., Mlawer, E.J., and Shippert, T.R., Observational determination of surface radiative forcing by CO_2 from 2000 to 2010. *Nature*, 519, 339–342 (2015).

7. Komori, S., Kurose, R., Takagaki, N., Ohtsubo, S., Iwano, K., Handa, K., Shimada, S., Sensible and latent heat transfer across the air-water interface in wind-driven turbulence, www.fluid.me.kyoto-u.ac.jp/members/kurose/komori_gtws2010_2011.pdf

SUPPLEMENT

9

SOME MASS TRANSFER ISSUES CONCERNING COVID-19

CONTENTS

1 Introduction 76
2 Droplet Evaporation and Deposition 76
3 Respirators and Masks 79
3.1 Respirators 79
3.2 Surgical Masks 80
3.3 Pressure Drop 80
3.4 Cloth Masks 81
3.5 The Epidemiology of Face Coverings for COVID-19 82
3.6 Recent Developments 84
3.7 Use of Two Masks 85

1 INTRODUCTION

The COVID-19 pandemic is causing worldwide havoc. Many aspects of spread of the novel coronavirus (SARS-CoV-2) are currently the subject of intensive research. Mass transfer processes play an important role in this research; this supplement is concerned with two topics. The first concerns transport of the virus. It is generally believed that one way the virus can be transmitted is by inhalation of droplets and aerosols emitted by an infected person when sneezing, coughing, singing, or simply talking and breathing. As a result the concept of *social distancing* is central to efforts to prevent the spread of infection. It is important to understand the nature of these emissions, for example the quantity and size distributions of the droplets and aerosols, and the subsequent transport processes. The general literature of the subject often has confusing statements concerning emissions and their characterization as droplets or aerosols. After ejection the droplets commence to evaporate: the rate of evaporation and droplet lifetime is a classic simultaneous heat and mass transfer problem that is dealt with in Chapter 1 of MT and Chapter 9 of BHMT. Part 2 of this supplement suggests how the textbook theory can be used to clarify aspects of the emissions behavior.

The second topic of this supplement concerns the performance of masks and respirators used to prevent transmission of emissions from and to the faces of medical personnel, patients in hospitals and nursing homes, service workers and the general public. A facial covering in termed a mask when its purpose is to prevent emissions from the wearer's mouth and nose from being transmitted to a nearby person or into the surrounding environment. That is, a mask is a *source control* to protect other people from a virus. On the other hand, a respirator has the purpose of preventing particles from reaching the face of the wearer for subsequent inhalation and is termed *personal protection equipment* (PPE). To some extent masks also act as respirators, but they are not really designed for this purpose. Masks and respirators are essentially fibrous filters. The applicable theory is developed in Chapter 3 of MT, section 3.3.4, and the accompanying software FILTER is useful for design calculations. It is usual for respirators to have a stage that is essentially an electrostatic precipitator. Section 3.3.3 of MT develops the theory of such equipment.

2 DROPLET EVAPORATION AND DEPOSITION

Human droplet emissions are characterized by a wide range of sizes. The general literature characterizes the droplets as large enough to deposit on surfaces by the action of gravity, or small enough to remain suspended in air and *float around* for some hours. The rate of droplet evaporation clearly plays a central role in this behavior, as was explored in an early study by Wells in 1934 [1], and more recently by Xie et al. in 2007 [2]. Two time scales characterize this problem: the time required for complete evaporation of a droplet, and the time required for a droplet to fall to the ground. A height of 2 m is often used for this purpose.

Example 1.10 of MT (9.10 of BHMT) examines the evaporation of a 50 μm diameter water droplet in an air stream using low mass transfer rate theory. In the

limit of Sherwood number equal to 2, the lifetime was derived as

$$\tau_e(\text{evaporation}) = \frac{\rho_l D_0^2}{8\rho \mathscr{D}_{12}(m_{1,s} - m_{1,e})} \tag{2}$$

Various assumptions in the analysis were evaluated including the duration of the initial temperature and velocity transients, and the neglect of radiation heat transfer. For a given temperature T_e and relative humidity RH_e, the diffusive wet bulb temperature equals the droplet temperature, and hence $m_{1,s}(P, T_{WB})$ is calculated for use in Eq. (2).

For the emissions we recognize that saliva is usually greater than 99% water: thus, for a preliminary model, a pure water droplet is assumed. Initially a droplet is surrounded by almost saturated air from the lungs and mouth, but this air then mixes with ambient air. Thus T_e and RH_e should be varied parametrically to explore possible evaporation times, which the need to be compared with the times required for a droplet to fall to the ground. Assuming Stokes drag law, the terminal velocity of a spherical droplet is

$$V_t = \frac{gD^2}{18\mu}(\rho_l - \rho_e) \tag{3}$$

and a lower limit on the fall time based on initial droplet size is

$$\tau_f^0 = \frac{2}{V_t(D_0)} \tag{4}$$

A sample result for $T_e = 25°\text{C}$, $\text{RH}_e = 65\%$ follows. The dramatic effect of $\tau_e \propto D_0^2$ and $\tau_f^0 \propto D_0^{-2}$ is clearly displayed.

$D_0(\mu\text{m})$	$\tau_e(s)$	$\tau_f^0(s)$
1	0.0008	6.8×10^4
2.5	0.005	1.1×10^4
5	0.02	2700
10	0.08	680
30	0.72	74
60	2.9	18.5
100	8	6.8
200	32	1.7
1000	800	0.068

Table 1: Evaporation and fall times of droplets, $T_e = 25°\text{C}$, $\text{RH}_e = 65\%$.

Consider first a 200 μm droplet: the actual value of τ_f is but a little longer than $\tau_f^0 = 1.7$s since $\tau_e = 32$s, i.e., there is only a small size change due to evaporation. On the other hand, for the 60 μm droplet, the value of $\tau_f^0 = 18.5$s is meaningless since the droplet has dehydrated at $\tau = 2.9$s. The diameter of droplet that is just completing evaporation when it reaches the ground is approximately 100 μm: the

exact value can be obtained by solving an appropriate ordinary differential equation for $D(t)$.

This sample calculation shows that the often seen conjecture that *small* droplets can remain suspended in air for minutes, even hours, is misleading. Even a 1000 μm droplet, which takes 13 min to evaporate, has fallen to the ground in 0.07s: it cannot simply *float around* in the stagnant air of the sample calculation.[1] So what can float around? It is the residue left when a saliva droplet has completely dehydrated: a mix of electrolytes, mucous, enzymes, antibacterial compounds, and of course virions if the source has a viral infection. But there have been few studies of these aerosols, and little is known about their physical characteristics.

A very recent and already often referenced experimental study is that of Stadnytskyi et al. PNAS May 13, 2020 [3]. A highly sensitive laser light scattering method revealed that loud speech can emit thousands of oral fluid droplets per second. The closed 0.6 m high test chamber contained stagnant air at $T_e = 23°\mathrm{C}$, $\mathrm{RH}_e = 27\%$. Droplet residence times were used to estimate an average fall velocity of 0.06 cm/s. Assuming that the droplets were falling at their terminal velocity for most of their residence time, they estimated a droplet diameter of $\sim 4\,\mu$m. They also estimated that the initial diameters of these droplets were 12–21 μm. For their air condition, Eqs. (2) and (4) give the following results $(T_e = 25°\mathrm{C}, \mathrm{RH}_e = 27\%)$

$D_0(\mu\mathrm{m})$	4	10	12	21
$\tau_e(s)$	0.016	0.1	0.144	0.44
$\tau_f^0(s)$	630	102	71	23

Since $\tau_e = 0.016$s for a 4 μm droplet, what was actually observed were 4 μm particles consisting of the residue left after evaporation. The estimated initial droplet diameter of 21 μm corresponds to a saliva water content of 99.3%, which is typical. Since τ_e for a 21 μm droplet is only 0.44s, the observed particles were always residue and not droplets. Thus their concluding statement that "normal speech generates airborne droplets that can remain suspended for tens of minutes or longer" is certainly misleading. It is also highly unlikely that droplets of size $O(0.1)\mu$m have been seen: such small particles are surely droplet residues after dehydration. These particles are often called droplet *nuclei*, which is also misleading. Respiration droplets result from rupturing and fragmentation of saliva in the mouth and respiratory tract: they are not formed by a nucleation processes such as those found in the formation of fog, mist or clouds.

There have been relatively few measurements of droplet size distributions for respiratory emissions because of the difficulties involved, and we do not have a reliable data base. Although a size range of 0.1 to 500 μm is often quoted, the size range of importance for COVID-19 transmission appears to be smaller, say 0.5–50 μm. This lack of knowledge hinders the development of useful physical models.

Another major uncertainty in predicting the role played by aerosols in COVID-19 transmission, is the quantity and lifetimes of virions in droplet residues, and their ability to cause infection. Hopefully, ongoing research will clarify these issues.

[1] Note that these calculations neglect convective air flow past the droplets. Such air flows, especially updrafts caused by air conditioning, could suspend a larger droplet for longer times than those associated with ballistic gravitational descent. Updrafts may be particularly relevant in confined spaces, such as elevators.

3 RESPIRATORS AND MASKS

The filters in modern respirators and surgical masks are of the fibrous type consisting of flat nonwoven mats of fine fibers. The physical processes by which a filter captures particles are described in Section 3.3.4 of MT, as is analysis of the performance of filters as single stream mass exchangers. The efficiency (effectiveness) of a filter is given by Eq. (3.25) as

$$\varepsilon = 1 - e^{-N_{\text{tu}}}; N_{\text{tu}} = \frac{4(1-\varepsilon_v)\gamma L}{\varepsilon_v \pi d_f} \tag{5}$$

where ε_v is the volume void fraction, γ is the single fiber collection efficiency, L is the filter thickness, and d_f is the fiber diameter. Table 3.2 gives recommended formulas for γ in terms of the pertinent flow and particle dimensionless parameters, including the Reynolds, Peclet, Interception and Stokes numbers. Equation 3.25 and Table 3.2 are incorporated in the software FILTER which facilitates design calculations. An alternative for mask filters is to specify a penetration $P = 1 - \varepsilon$ rather than the effectiveness ε.

Current practice is to use nonwoven polypropylene fiber mats in multiple layers. A typical respirator has two spun-bonded outer layers, to protect against the outside environment on one side and to serve as a barrier to the wearer's emissions on the other. Between the outer layers is a pre-filtration layer to trap larger particles, and the filtration layer that controls the filter performance. The *filtration* layer is not a simple fibrous filter, but has charged fibers to facilitate particle deposition by electrostatic precipitation. The fibers are dielectric and have permanent positive and negative charges; they are called *electret* filters. The term electret is analogous to the term *magnet* for permanent magnetic fields. Electrostatic precipitators are dealt with in Section 3.3.3 of MT: the basic physics is described and design principles given for the large precipitators used in power plants and for incinerators. Single fiber collection efficiency is critically dependent on particle size. Without electrostatic precipitation this efficiency has a minimum for particle sizes in the vicinity of 0.3 μm, which is an important size for medical filters to deal with. Electrostatic precipitation is effective over a wide range of particle sizes relevant to medical filters and plays an important role in increasing respirator performance.

3.1 Respirators

There is a great variety of masks and respirators in common use. For example, Balazy et al. [4] tested a 3 layer respirator with this specification:

	L(mm)	$d_f(\mu$m)	ε_v
External layer	0.31	39.5	0.835
Middle layer	1.77	7.8	0.931
Inner layer	1.05	40.9	0.80

The middle layer is an electret medium. To illustrate the role played by electrostatic deposition, the software FILTER can be used to estimate the expected performance without electrostatic deposition. Choosing $\rho_p = 1000$ kg/m^3, $V = 0.1$ m/s,

$P = 1$ atm, $T = 300$ K, FILTER gives the following result.

d_p, μm	0.03	0.05	0.1	0.3	0.5	1.0	3.0	10
ε	0.77	0.542	0.289	0.103	0.074	0.071	0.536	1.0

The universal standard for respirators in the medical field is the N95, or equivalent, mask. The N designation simply refers to *Non-oil* meaning in environments where no oil-based particulates are present. The value 95 is the percent efficiency of the mask for 0.3 μm particles. As noted before, single particle collection efficiency tends to have a minimum in the vicinity of 0.3 μm: at smaller sizes, collection by diffusion rapidly becomes more effective. The Balagy filter is intended to meet N95 performance: clearly it must rely on electrostatic collection in order to do so.

3.2 Surgical Masks

The main purpose of surgical masks is to prevent doctor or nurse emissions of saliva droplets from impinging on the patient, especially on open wounds. Filtering of aerosols, which may be very small droplets or droplet residues, is a secondary objective. These masks are not designed to efficiently prevent aerosols from reaching the user's face. Often they are loose fitting, so inhaled air preferably bypasses the filter by flowing through gaps between the mask and face. On the other hand, respirators are required to fit tightly on the user's face to have a good seal. The fitting process is an essential routine in hospitals. A proper surgical mask is usually made of three layers including an outer hydrophobic nonwoven layer, a middle melt-blown layer, and an inner soft absorbent nonwoven layer.

Performance of surgical masks involves many issues: filtration involving capture of both exhaled and incoming aerosols, air flow resistance, water repellancy for inner and outer surfaces, and water vapor and air permeability. For example, in the U.S. the bacterial filtration efficiency (BFE) is required to be $>95\%$ for 3μm particles. Surgical masks do not have an electret filter layer and thus have collection efficiencies lower than for N95 respirators in the particle size range 0.1–1 μm. Performance data are sparse and not well documented. Konda et al. [10] give values of 0.4–0.6 for 0.3 μm particles, but lower and higher values are also reported. Since surgical masks are loose fitting, the quality of fit plays an important role, particularly at higher breathing rates. Konda et al. [10] report values below 0.2 at higher flow rates. It is important to remember that surgical masks were not developed for personal protection, i.e., as respirators. Their performance as respirators has become more important only due the recent shortage of N95 units, which has required medical workers to substitute the masks for N95 units.

3.3 Pressure Drop

As with all mass exchangers, the pressure drop across the filter is an important factor. For industrial equipment the cost of the fan power required is as important design constraint. For medical masks and respirators the criterion relates to the comfort of the users when inhaling and exhaling. The Handbook of Nonwoven Filter Media by Irwin. M. Hutten [5] has an extensive treatment of flow through nonwoven media. Many theories have been proposed to model the flow: for example, Kuwabara [5]

Table 2: Pressure drop for flat electret filters

Media Type	Basis Weight g/m^2	Thickness mm	Pressure Drop Pa	Fiber diameter μm
Fibrillated polypropylene film	100	2.4	0.7	22
Electrostatic charged polypropylene BMF	60	0.9	3.2	8
N-type advance electret	60	0.9	3.0	8
R-type advance electret	60	0.9	2.8	8
P-type advance electret	60	1.0	3.8	7

derived

$$\frac{\Delta P d_f^2}{\mu V L} = \frac{16\varepsilon_v}{H} \tag{6}$$

where V is the superficial flow velocity, and H is the hydrodynamic factor for Kuwabara flow, given in Table 3.2 of MT. Respirator filters must meet stringent certification tests established by NIOSH (The National Institute for Occupational Safety and Health) in 42 CFR Part 84 "Respiratory Protective Devices". Air flow testing is done with 85 l/min on a surface area of 182 cm^2, a velocity of 7.8 cm/s. The initial breathing resistance to air flow must not exceed 350 Pa and initial exhalation resistance is not to exceed 250 Pa.

Barrett and Rousseau [6] measured pressure drop for flat sheets of electret filter material; their data is in Table 2. Basis weight is the filter weight per unit with surface area. These low viscous pressure drops for the filter layer implies that pressure drop across a mask is dominated by inviscid pressure drop components.

3.4 Cloth Masks

Partly due to the early lack of availability of N95 and surgical masks, cloth masks are now in very wide use in the U.S. Cloth masks can be used as a replacement for surgical masks, i.e., as a *source control* to reduce disease transmission by the wearer's respiratory droplets. But generally they have a low filter efficiency (varying from 2 to 46%) and are not considered as satisfactory personal protective equipment (PPE) for the wearer. There are no standards or regulations for home-made cloth masks [7]. However, one useful feature of cloth masks is easy cleaning in a washing machine. The more complex cleaning/replacing protocols for more advanced masks discourages their proper execution.

Table 3 lists test results for commonly used homemade mask materials: the test procedure was the same as that used to give N95 respirators their NIOSH certification, by TSI. Inc. [8]. The test superficial face velocity was $\sim$ 10 cm/s. Actually, materials such as natural silk, polyester-Spandex, and flannel can likely provide some electrostatic filtering.

The work of Rengasamy et al. [9] is particularly useful because they tested monodisperse aerosols over the size range 0.02–1 μm for three different commercial

Material	Pressure Drop [Pa]	Efficiency [%]
2 layers Kona 100% Quilters cotton	65	7.0
Folded Bandana	34	9.7
Broadcloth Polyester blend	96	11.4
Duck canvas	92	13.7
1 layer Kona, 1 layer flannel	84	15.4
3 layer Hanes cotton T-shirt	89	28.0
2 layer Wypall towels $\times$ 80	61	30.6
2 layer Toolbox towels	120	42.0
1 layer Zep, 1 layer Toolbox, towel	116	55.7
1 layer Filti, 1 layer 6.5 g cotton Rip stop*	13	84.0

*Filti face mask material is a polypropylene spunbound nonwoven with a nano fiber fine filtration layer and a surface layer of polyester nonwoven. It is readily available for homemade masks.

Table 3: Pressure Drop and Efficiency for mask materials

face mask materials, sweat shirts, T-shirts, towels and scarves. The results are presented as % penetration, rather than efficiency. Clear comparisons with N-95 media are shown. For the important 0.3 μm size, efficiency was generally 10–20%: a fleece mask gave the highest value of about 25%. In practice these values will be lower because of fit issues.

Because of the low efficiency of most cloth masks they are not generally recommended as personal protection equipment. On the other hand, cloth masks are attractive for source control. A cloth mask is usually able to intercept the larger droplets emitted by an infected wearer, and these droplets would contain most of the virons. The smaller aerosol sized droplets that are not filtered contain but a small fraction of the volume of emitted saliva.

A recent review of masks and respirators has been given by Brosseau and Sietsema [11]. The thrust of the review is conveyed by its title: "Masks-for-all for COVID-19 is not based on sound data". They do not recommend requiring the general public who do not have symptoms of COVID-19 like illness to routinely wear cloth or surgical masks. This view point is controversial.

3.5 The Epidemiology of Face Coverings for COVID-19

In previous sections of §3 the performance of face coverings was explored based on the physics/engineering of their performance as mass exchangers. This approach allowed us to look at issues such as the effects of filter parameters including fiber diameter and volume void fraction, and particle size, as well as flow parameters. Experimental data for filter efficiency was reviewed. In principle this approach leads to the proper design of masks and respirators to yield a specified performance. The desired end results are policy recommendations for the use of masks by medical personnel and, in the case of a pandemic, for the general population.

However, there is a completely different approach to the issues of concern that is used by public health workers. It is based on epidemiology, i.e., that branch or medicine which deals with the incidence, distribution and possible control of disease and health conditions. A very recent and pertinent epidemiological study of the transmission of COVID-19 has been published by Zhang et al. [12]. By analyzing the trend and mitigation data for Wuhan, Italy and New York city they found that the difference with and without mandated face coverings "represents the determinant in shaping the pandemic trends in these epicenters". They claim that this mitigation measure alone reduced the number of infections by over 78,000 in Italy from April 6 to May 9, and by over 66,000 in New York City from April 17 to May 9. Such dramatic results have encouraged public health agencies to require wearing of face coverings in public, or when social distancing cannot be practiced.

This epidemiological study cannot, in principle, inform that the result is due to the masks acting as source controls, personal protection equipment (PPE) or both. To answer this question we can look at data for the performance of surgical and cloth masks as PPE that is, their efficiency in filtering aerosols that might transport COVID-19 virons to the mouth and nose. As discussed in Sections 3.2 and 3.4, both surgical and cloth masks are not recommended by the responsible agencies for use as PPE: their efficiency is too low. Thus we conclude that the Zhang et al. result indicates that surgical and cloth masks must be effective source controls. Emitted droplets can have a large range of sizes, from 1 to 500 μm according to Stadnytkski et al. [3]. Human coughing produces droplet sizes in the range 0.62–15.9 μm, with an average mode size of 8.35 μm [13]. Sneezing produces droplet sizes that are much larger. Han et al. [14] found both unimodal and bimodal size distributions, with geometric mean sizes of 360 μm and 74 μm, respectively. Thus nearly all emitted saliva is in droplets that will deposit in filters by being blocked or by inertial impaction, and the corresponding filter efficiencies for surgical and cloth masks will be high. The results of the epidemiological study and the basic physics of the operation of surgical and cloth masks are thus compatible.

Surprisingly, there is very little useful data for masks acting as source controls. The recent paper by Fischer et al. [15] attempts to remedy this situation, but has limited value. Only numbers of droplets/droplet residues that were transmitted by the mask were measured. Since the number of virons in a droplet depends on its volume, the droplet size plays an important role. Each mask material will change the size distribution in a different way. The student can use FILTER to explore the effect of parameters such as fiber diameter and volume void fraction in the example given in Section 3.1 to explore this issue. Lustig et al. [16] claim to be concerned with masks as PPE, but an examination of their experimental rig and procedures suggests a situation more applicable to source control. Their challenge droplet size distribution was chosen to match forceful expiration, that is, pertinent to source control, not a size distribution that would match conditions in, for example, an indoor room where large droplets have settled out by gravity, and evaporation has radically changed the sizes of smaller droplets and yielded droplet residues. Their experimental procedure also fails to recognize that evaporation of saliva droplets yields a solid residue far larger than individual virions contained therein. Their data for transmission of virion size particles is thus not pertinent to the real problem, and should be disregarded. Further research on this important topic is clearly necessary

Three last comments on surgical and cloth masks are relevant.

1. Many users are simply unaware that these masks do not qualify to be PPE. As a result the user may have a false sense of security, and be less diligent in practicing social distancing and hand washing.
2. Why do we require the general population to wear surgical or cloth masks? It is because our hypothesis is that anyone is possibly infected with COVID-19. Thus when masks are removed they have to be treated as being contaminated with the virus and cleaned or disposed of accordingly. A used mask from an infected person will be very dangerous.
3. Following on (2) above. When exercising outdoors and following social distancing guidelines, mask wearing is likely to be counterproductive. Firstly, it is not healthy as it may interfere with the respiratory function, especially for physical activities that result in heavy breathing.[2] Secondly the mask of an infected person after exercising will be saturated with virons and be dangerous to contact. Far better the virons be allowed to escape to the open air while exercising!

3.6 Recent Developments

Aydin et al. [17] at the University of Illinois [17] have conducted an experimental study to determine the performance of cloth masks as source controls.The experimental procedure attempts to mimic conditions characteristic of human emissions (coughs, sneezes and speech), which produce saliva droplets up to 1 mm in size, as well as aerosols of size less than 5-10 micrometers impinging on the inside of a mask. Previous tests of cloth masks focussed on the masks as PPE, and used dry aerosols in the size range 0.02-5.0 micrometers [9,10], as discussed in Section 3.2 and 3.4. However, most of the saliva volume (including virions in the case of an infection) is contained in relatively large droplets. [18] measured a droplet size distribution for normal speaking that gave a geometric mean diameter of 16.0 micrometers with a size range of 2-1000 micrometers. Of particular importance is that 99.5% of the saliva volume was contained in droplets larger than 100 microns. The fabrics tested typically had pore sizes about 30-60 micrometers: hence the essential physics for source control is not described by filtration theory. The primary function of the fabric is to block droplets larger than the pore size. As Aydin et al. show, the subsequent droplet liquid transmission through the mask depends on whether the fabric is hydrophilic or hydrophobic, the pore size and porosity, and the droplet liquid viscosity. The concept of a filtration efficiency is replaced by a volumetric blocking efficiency. Testing used droplets with diameters 0.12-1.33 mm, with a median of 0.28 mm [17]. A non-woven polypropylene medical mask was tested to give reference data, yielding a median blocking efficiency of 98.5%.The various fabrics tested gave values from 71.7-98.7%. Using multiple layers gave higher values, up to 98.9% for 3 layers of used shirt. These high values of blocking efficiency support claims that medical and cloth masks can be very effective source controls. Current government policy requiring their use is thus well supported by the applicable science. Aydin et al. [17] is a landmark contribution in that it is the

[2] Given that there is evidence that many COVID-19 spreaders are unaware of their own infection, the importance of observing enhanced social distancing protocols around people who are exhaling strenuously cannot be overestimated.

first to clearly identify the mechanisms involved when masks act as source controls, and to demonstrate the importance of droplet blocking, wetting behavior and liquid flow in determining mask performance. Previously, research has focused on aerosol filtration, often without being aware that filtration is only relevant to masks used as PPE. As noted in Section 3.4, cloth masks do not perform well as PPE because of their low filtration efficiency for the important 0.1-1.0 micron particle size range. We can expect to see much research activity building on this pioneering work.

3.7 Use of Two Masks

There is current media discussion supporting the use of two masks to give improved protection. Dr. Faucci has been quoted to say it was *common sense* that two masks would improve protection. Implicit in this discussion is that PPE is the focus, for which Eq. (5) gives the filtration efficiency. The negative exponential dependence on thickness implies that use of two masks will make sense only if they individual efficiencies are low or if the additional mask improves fitting to the face. A properly fitted N95 mask exceeds 95% efficiency: adding another mask can give but a small increase in filtration. Test data of Konda et al. [[10]] show that for high efficiency masks, it is more important to focus on having a good fit, rather than adding more Ntu. A simple way to improve the mask fit is to wear a nylon stocking as an outer layer to hold the mask tightly against the face. Mueller et al. [19] present encouraging results for this approach.

However, in Section 3.5 we argued that the major benefit of mask wearing for the general public is as source control, not as PPE. Aydin et al. [17] have shown cloth mask blocking efficiencies are in the range of 70-98%,with the majority of the fabrics giving values greater than 90%. So again, adding a second mask will not give a significant increase in blocking efficiency unless the additional mask improves the fit to the face. Valid test data for masks acting as source control are very limited, and further research is indicated.

Another issue related to use of multiple masks is the increase in pressure drop, and its impact on wearer comfort. Pressure drop for masks acting as PPE was discussed in Section 3.3. Table 3 gave pressure drops for cloth masks at a test superficial velocity of $\sim$10 cm/s, corresponding to NIOSH testing for N95 masks. Section 3.4 discussed flow through nonwoven media, and Table 2 gave pressure drop data for flat electret filters: values are more than an order of magnitude less than for cloth masks. Aydin et al. [17] present pressure drop data by defining a *breathability* β equal to superficial velocity/pressure drop. They obtained 1.83 (m/s)/Pa for a medical mask. At their test condition this corresponded to a pressure drop of 55 Pa. For three layers of a T-shirt fabric, $\beta = 2.03$ (mm/s)/Pa giving pressure drop of 38 Pa. This value is roughly comparable to those in Table 3. But for source control the flow is droplet laden, and the droplets blocked by the fabric will certainly affect pressure drop. This issue requires further attention.

REFERENCES

1. Wells, W.F., "On airborne infection," American. J. Epidemiology, 20, 611–618 (1934)
2. Xie, X. et al. "How far droplets can move in indoor environments-revisiting the Wells evaporation-falling curves," Indoor Air, 17, 211–225 (2007)
3. Stadnytski, V., Bay, C.E., Bax, A., and Anfinrud, P., "The airborne lifetime of small speech droplets and their potential importance in SARS-CoV-2 transmission," PNAS 2006874117 (2020)
4. Balazy, A. et al. "Manikin-Based Performance Evaluation of N95 Filtering-Face piece Respirators Challenged with Nano particles," Annals of Occupational Hygiene, 50, 259–269 (2006)
5. Hutten, I.M.M., *Handbook of Nonwoven Filter Media*, Elsevier, 2007.
6. Barret, L.W., and Rousseau, A.O., "Aerosol Loading Performance of Electret Filter Media," AIHI Journal, 59, 532 (1998)
7. Wikipedia, Cloth face masks
8. DYI MASK FAQ, https://www.maskfaq.com/test-results
9. Rengasamy, S., Eimer, B., and Shaffer, R.E., "Simple respiratory protection – evaluation of the filtration performance of cloth masks and common fabric materials against 20–1000 nm size particles," Annals Occupational Hygiene, 54, 789–798 (2010)
10. Konda, A., et al. "Aerosol filtration efficiency of common fabrics used in respiratory cloth masks," ACS Nano 145, 6339–6347 (2020)
11. Brosseau, L.M., and Sietsema, M. "Commentary: Masks for all for COVID-19 not based on sound data" https://www.cidrap.umn.edu/news-perspective/2020/04/commentary-masks-for-all-covid-19.not-based-on-sound-data.
12. Zhang, R., Li, X., Zhang, A.L., Wang, Y and Molina, M.S., "Identifying airborne transmission as the dominant route for the spread of COVID-19," PNAS June 30, 2020 117(26) 14857–14863.
13. Yang, S. et al. "The size and concentration of droplets generated by coughing in human subjects,' J. Aerosol Medicine, 20, 484–494 (2007)
14. Han, Z.Y., Weng, W.G. and Huang, Q.Y., "Characteristics of particle size distribution of the droplets exhaled by sneeze," J.R. Soc Interface 10: 20130560. http://dx.doi.org/10.1098/rsif.2013.0560 (2013)
15. Fischer, E.P. et al. "Low-cost measurement of face mask efficacy for filtering expelled droplets during speech," Science Advances, DOI: 10.1126/sciadv.abd308307 Aug. (2020).

16. Lustig, S.R. et al. "Effectiveness of common fabrics to block aqueous aerosols of virus-like nanoparticles," ACS Nano, 14, 7651–7658 (2020).

17. Aydin, O. et al. "Performance of fabrics for home-made masks against the spread of COVID-19 through droplets: A quantitative mechanistic study," Extreme Mechanics Letters, 40, 100924 (2020).

18. Chao, C.Y.H. et al. "Characterization of expiration air jets and droplet size distributions immediately at the mouth opening," J.Aerosol Sci.40 (2),122-133 (2009).

19. [19] Mueller, A.V. et al. "Quantitative method for comparative assessment of particulate filtration efficiency of fabric masks as alternatives to standard surgical masks for PPE" Matter 3 (3), pp. 950-962. doi:10.1016/j.matt.2020.07.006.